

11-30-2007

Characterization and Mitigation of Hyper-Rayleigh Fading

Richard Ketcham
University of Vermont

Follow this and additional works at: <http://scholarworks.uvm.edu/graddis>

Recommended Citation

Ketcham, Richard, "Characterization and Mitigation of Hyper-Rayleigh Fading" (2007). *Graduate College Dissertations and Theses*. Paper 121.

This Thesis is brought to you for free and open access by the Dissertations and Theses at ScholarWorks @ UVM. It has been accepted for inclusion in Graduate College Dissertations and Theses by an authorized administrator of ScholarWorks @ UVM. For more information, please contact donna.omalley@uvm.edu.

CHARACTERIZATION AND MITIGATION OF HYPER-RAYLEIGH FADING

A Thesis Presented

by

Richard Patrick Ketcham

to

The Faculty of the Graduate College

of

The University of Vermont

In Partial Fulfillment of the Requirements
for the Degree of Master of Science
Specializing in Electrical Engineering

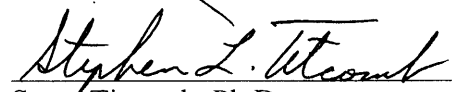
October, 2007

Accepted by the Faculty of the Graduate College, The University of Vermont, in partial fulfillment of the requirements for the degree of Master of Science, specializing in Electrical Engineering.

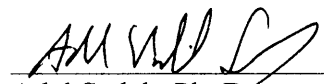
Thesis Examination Committee:



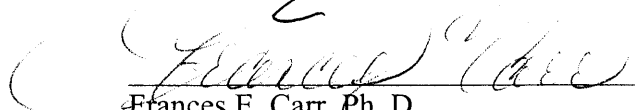
Jeff Frolik, Ph.D. **Advisor**



Steve Titcomb, Ph.D.



Adel Sadek, Ph. D. **Chairperson**



Frances E. Carr, Ph. D. **Vice President for Research
and Dean of Graduate Studies**

Date: August 21, 2007

ABSTRACT

Due to the unprecedented spatial and temporal resolution they offer, wireless sensor networks are considered an enabling technology for the distributed monitoring of industrial, military, and natural environments. As these systems migrate into vastly different and novel applications, new constraints are discovered that affect network reliability and utility. For example, wireless sensors are typically statically deployed and, unlike mobile systems, cannot move to a new location for better radio reception. As a result, the signal fades caused by non-optimal environmental conditions can increase the outage probability of the system, potentially rendering the network unreliable and ineffectual. Stochastic models that quantify link reliability and the effectiveness of diversity methods are often employed to understand the impact of such fading. However, the performance of these models applied to wireless sensor networks is entirely dependent on the appropriateness of the model with respect to the environment.

This work first presents an empirical study of the propagation environment for a wingless, rotary aircraft, showing that the wireless environment within exhibits frequency-selective fading much more severe than predicted by current worst-case models (i.e., Rayleigh). An analysis is then given of the effectiveness of several diversity methods operating within such environments (referred to as hyper-Rayleigh). These fade mitigation techniques are simple enough to be employed for use with low-complexity wireless sensor hardware, and include spatial diversity, polar diversity, two-element passive combining, and two-element phased combining. Two-element phased combining is further developed by examining the effect that smaller element spacing has on diversity gain. A demonstration of a wireless sensor utilizing such a two-element phased combining antenna is described in detail.

ACKNOWLEDGEMENTS

I would like to thank my family, Mom, Pop, Meg, and Dave - as well as Amanda Daly - who, with love and understanding, have helped me through the arduous process known as graduate school. I would also like to thank John Covell and Bob Zelif of Goodrich for their insight and support. Most of all, I want to thank Dr. Jeff Frolik for his outstanding mentorship, ability to inspire and engage, and the incalculable effect his guidance has had on me as a student, and as an engineer.

CITATIONS

Material from this thesis has been submitted for publication to Transactions on Aerospace and Electronic Systems on November 26, 2006 in the following form:

Ketcham, R., J. Frolik, and J. Covell, "Propagation characterization for in-aircraft wireless sensor systems," Transactions on Aerospace and Electronic Systems.

Material from this thesis has appeared in the following forums:

Ketcham, R., J. Frolik, S. Melais, and T. Weller, "Effectiveness of simple diversity methods in mitigating hyper-Rayleigh fading environments," 2006 IEEE Wireless and Microwave Conference, December 4-5.

Ketcham, R., and J. Frolik, "A Low-Complexity, Compact Antenna for Mitigating Frequency Selective Fading," Sixth International Conference on Information Processing in Sensor Networks (IPSN07), Boston, MA, May, 2007.

TABLE OF CONTENTS

	Page
ACKNOWLEDGEMENTS.....	ii
CITATIONS	iii
LIST OF TABLES.....	viii
LIST OF FIGURES	ix
CHAPTER 1: INTRODUCTION	1
1.1 Motivation.....	1
1.2 Problem Statement.....	2
1.3 Thesis Contributions.....	4
1.4 Thesis Outline	5
1.5 References.....	6
CHAPTER 2: SMALL-SCALE PROPAGATION MODELING	8
2.1 Propagation Phenomenon	8
2.2 Physical Underpinnings of Common Small-Scale Fading Models	9
2.3 Modeling Hyper-Rayleigh Fading.....	18

2.4	Cumulative Distribution Function (CDF).....	21
2.5	Conclusions.....	26
2.6	References.....	27
CHAPTER 3: PROPAGATION CHARACTERIZATION FOR IN-AIRCRAFT WIRELESS SENSOR SYSTEMS.....		28
3.1	Foreword.....	28
3.2	Propagation Characterization for in-Aircraft Wireless Sensor Systems.....	28
3.3	Test Methodology	31
3.4	Results and Discussion	40
3.5	Conclusions.....	46
3.6	References.....	47
CHAPTER 4: COMPACT AND SIMPLE DIVERSITY METHODS FOR MITIGATING SEVERE FADING		49
4.1	Foreword.....	49
4.2	Compact and Simple Diversity Methods for Mitigating Severe Fading	49
4.3	Spatial/Polarization Diversity Gains.....	52
4.4	Coarse Phase Combining Gains.....	56

4.5	Conclusions.....	59
4.6	References.....	60
CHAPTER 5: RESULTS FROM ADDITIONAL ANTENNAS		61
5.1	Passive Combining with $\lambda/2$ Element Spacing.....	61
5.2	Coarse Phase Combining with $\lambda/4$ Element Spacing	66
5.2	Conclusion.....	70
CHAPTER 6: INTEGRATING A DIVERSITY ANTENNA WITH HARDWARE ...		71
6.1	Foreword.....	71
6.2	Integrating a Diversity Antenna with Hardware.....	71
6.3	Diversity Antenna Design.....	73
6.4	Demonstration Overview.....	74
6.5	Demonstration Details	76
6.7	Demonstration of Graphic User Interface.....	77
6.8	References.....	78
CHAPTER 7: CONCLUSION AND EXTENSIONS TO WORK.....		79
7.1	Significant Contributions of Work	79

7.2	Current Work: CRCE Chamber.....	80
7.3	Future Work with Coarse Phase Combining.....	86
7.4	Final Comments.....	87
7.5	References.....	88
	COMPREHENSIVE BIBLIOGRAPHY.....	90
	APPENDICES.....	93
	APPENDIX A: ANTENNA CONFIGURATION FOR CHAPTER 3 TESTS.....	93
	APPENDIX B: THEORETICAL GAIN EQUATIONS FOR CHAPTER 4.....	94
	APPENDIX C: POWER SUPPLY DESIGN FOR CHAPTER 6.....	96

LIST OF TABLES

Table	Page
Table 2.1. Fading behavior as defined by Δ and K factors.	20
Table 3.1. Test location features	32
Table 3.2. ISM bands characterized.....	33
Table 3.3. Summary of path loss data.....	41
Table 3.4. Fading classification criteria.....	42
Table 3.5. Classification of fading measurements conducted for the 915 MHz ISM band	43
Table 3.6. Classification of fading measurements conducted for the 2.4 GHz ISM band	43
Table 3.7. Classification of fading measurements conducted for the 5 GHz ISM band...	43
Table 4.1. Spatial diversity gains for mitigating measured severe fades.....	55
Table 4.2. Theoretical spatial diversity gains in Rayleigh environments	55
Table 4.3. Polarization selection diversity gains for mitigating measured severe fades ..	56
Table 4.4. Phase shifts required to mitigate severe fades	59
Table 5.1. Selection diversity and passive combining.....	64
Table 5.2. Channel characteristics for the right, left, and combined paths.....	64
Table 5.3. Average gain for the quarter wavelength antenna	69
Table 5.4. Average gain for the half wavelength antenna	69
Table A.1. Small- and medium-scale test hub positions.....	93

LIST OF FIGURES

Figure	Page
Figure 1.1. Illustration of possible wireless sensor network topologies.....	2
Figure 2.1. Ricean Fading Scenario.....	10
Figure 2.2. Rayleigh Fading Scenario.....	12
Figure 2.3. Hyper-Rayleigh Fading.....	18
Figure 2.4. CDF of Rayleigh and two ray fading.....	24
Figure 2.5. CDFs of the common fading models and hyper-Rayleigh fading.....	25
Figure 3.1. Test locations within transport helicopter.....	32
Figure 3.2. Measurement setup for test location ‘C’.....	33
Figure 3.3. Example frequency response (dB vs. Hz) taken at the passenger bulkhead (position ‘E’).....	34
Figure 3.4. Utilization of CDF curve to categorize small-scale fading. The response presented in Figure 3.3 is seen to exhibit hyper-Rayleigh fading statistics.....	39
Figure 3.5. Frequency-selective fading within passenger bulkhead exhibiting (<i>Trace 1</i>) Ricean, (<i>Trace 2</i>) Rayleigh, and (<i>Trace 3</i>) hyper-Rayleigh characteristics.	44
Figure 3.6. <i>CDF</i> curves for frequency selective fading measurements depicted in Figure 3.5.....	44
Figure 3.7. Example measurement (location ‘D’) exhibiting severe frequency-selective fading.....	45
Figure 3.8. CDF of Figure 3.7 exhibiting two-ray fading statistics.....	46
Figure 4.1. Spectrum and <i>CDF</i> depicting hyper-Rayleigh fading.....	54
Figure 4.2. The deep (~38 dB) fade disappears when the received antenna is moved by 1 cm. At this location the fading now exhibits Ricean statistics.	54
Figure 4.3. Simple two-element array utilized for coarse phase combining study.....	57
Figure 4.4. Two element antenna array with 0° phase shift.....	58
Figure 4.5. Two element antenna array with 180° phase shift on one element.....	59

Figure 5.1. Passive combining with $\lambda/2$ element spacing	62
Figure 5.2. Simulated diversity gains	62
Figure 5.3. Two element passive antenna (right element)	65
Figure 5.4. Two element passive antenna (left element)	65
Figure 5.5. Two element passive antenna (combined path).....	65
Figure 5.6. Prototype antenna with $\lambda/4$ separation	67
Figure 5.7. Quarter wavelength test components (power supply, controller, and antenna)	68
Figure 6.1. Freescale MC13192-EVB	73
Figure 6.2. Low-complexity diversity antenna	73
Figure 6.3. SPOTS demonstration routine	74
Figure 6.4. IPSN graphic user interface.....	75
Figure 6.5. Example frequency selective fading.....	75
Figure 7.2. Anechoic chamber testing a horn antenna.....	82
Figure 7.3. Reverberation chamber Otto-von-Guericke University, Germany	83
Figure 7.4. Fabricated CRCE with oscillating fan.....	84
Figure 7.5. Frequency-selective fading response exhibiting Rician characteristics. In-band plot (left) and CDF plot (right).	84
Figure 7.6. Frequency-selective fading response exhibiting Rayleigh-like characteristics. In-band plot (left) and CDF plot (right).....	85
Figure 7.7. Frequency-selective fading response exhibiting hyper-Rayleigh characteristics. In-band plot (left) and CDF plot (right).	85
Figure 7.1. Prototype antenna with zero separation.....	87
Figure B.1. Two element selection diversity fade probability.....	95
Figure C.1. Three power supply generations (oldest to newest, from left to right).....	97
Figure C.2. Latest version of antenna power supply	97
Figure C.3. Power supply circuit board	98
Figure C.4. Schematic for power supply in C.3.....	99

CHAPTER 1: INTRODUCTION

1.1 Motivation

In recent years, the diverse potential applications for wireless sensor networks (WSN) have been touted by both researchers and the press [1, 2, 3]. The utility of a WSN lies in its ability to monitor multiple variables (e.g. temperature, magnetic fields, vibration, etc.) over time at many locations, potentially distributed across a broad area.

In general, wireless sensor networks are seen as an enabling technology for distributed monitoring of industrial, military, and natural environments due to the unprecedented spatial and temporal resolution they offer. In industry, WSN streamline manufacturing processes by monitoring process variables and controlling their influence [4, 5, 6]. Within civilian areas, WSN are finding applications relating to health care [7], traffic control [8, 9], and home automation [10, 11]. Wireless sensor networks are also used in monitoring sensitive natural environments and are expected to yield long term data for analysis while reducing or eliminating the impact of observers on the phenomena being monitored [12, 13].

As WSN migrate into vastly different applications, issues adversely affecting the networks' reliability and utility arise with increasing frequency. Communication link connectivity, for example, is a shortcoming of many existing deployments. In particular, new WSN intended to operate within metallic cavities (e.g., airframes and shipping containers) have a likelihood of experiencing severe frequency-selective fading (also known as multipath) greater than that of worst-case models presently used.

1.2 Problem Statement

The utility of a WSN depends in part on the reliability of the wireless communication link between the sensor nodes, which is itself determined by the large- and small-scale fading characteristics of the environment. Small-scale effects (detailed in Chapter 2) for mobile communications are usually described using statistical models such as the Ricean and Rayleigh fading models. Our work has shown, however, that channel fading in some WSN environments may be more severe than predicted by these existing fading models, necessitating further study of propagation characteristics in such settings. Designing the WSN according to an appropriate model is requisite to ensure reliability of the system. Otherwise, the outage probability of a wireless system exceeds the desired system requirement, potentially rendering the WSN unreliable and ineffectual.

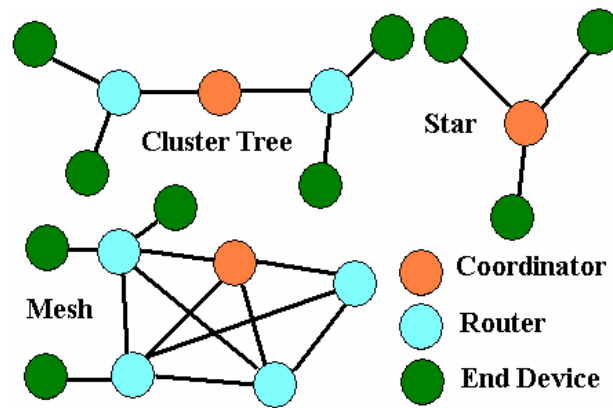


Figure 1.1. Illustration of possible wireless sensor network topologies

In a WSN, data may be routed through several nodes to extend the coverage area making the probability of successful communication from end to end dependent on the multiplicative probabilities of each individual link within the path. Figure 1.1 illustrates

three common topologies for wireless sensor networks. The simplest of the three topologies is the star network, in which all nodes - other than the coordinator (base-station) - are end devices and are within one transmission (hop) of the coordinator. Slightly more complicated is the cluster tree which essentially connects several individual star topologies to a common coordinator. In this configuration, the end devices are within two hops of the coordinator. The third and most complicated of the three topologies is the mesh network which allows data to take one or more hops to route to the coordinator. The nodes are usually distributed over a wide area and all depend on the propagation behavior of the wireless links between one another. The consequence of low link reliability is in the amount of energy required to overcome it. In many situations, a failed transmission in a WSN necessitates that the message be retransmitted until a successful transmission occurs. In most cases each node has a finite amount of energy, defined by the capacity of its battery, making retransmission a particularly distasteful solution to low link reliability. As such, it is important to minimize the retransmission rate, a process which requires that the channels first be modeled. A wireless link may traverse a large number of unique and independent paths, so it may be useful to model the channel using a statistical approach.

The challenge of using an appropriate fading model aside, wireless systems may experience fade severity that cannot be coped with simply by designing fade margins into the WSN. Instead, diversity strategies may be employed to mitigate severe fades that would otherwise jeopardize system reliability. In WSN, diversity techniques consist of transmitting the same information via multiple routes in an effort to improve reliability.

To our knowledge, the exploration of diversity strategies in conjunction with WSN, specifically within severe fading environments, has been minimal.

1.3 Thesis Contributions

The work herein investigates two problems yet to be addressed for wireless sensors deployed in severe fading environments. Specifically, these are 1) determining the potential severity of fades, and 2) developing practical schemes to mitigate them. The main contributions of the thesis are as follows:

- *Confirming the existence of severe frequency selective-fading through in-aircraft propagation studies.*

A study is presented in Chapter 3 which highlights that the fading experienced within aircraft is often much worse than predicted by the Rayleigh fading model. This regime of severe fading, referred herein as hyper-Rayleigh fading [14], is motivation to investigate mitigation methods for fades experienced by wireless sensors operating in such environments.

- *Examining the diversity gains achieved through the use of simple diversity methods in the presence of severe multipath fading.*

There is a long history of work conducted on the diversity gain of simple diversity methods within Rayleigh environments [15]. Chapter 4 demonstrates that, when fading is hyper-Rayleigh, our empirical diversity gains are greater than those predicted for Rayleigh environments.

- *Studying the diversity benefit for simple diversity antennas utilizing extremely small form factors.*

Wireless sensor nodes are necessarily small to remain unobtrusive while in operation. As such, it is of interest to use diversity techniques that take up little space. Unfortunately, using a smaller form factor is not without its consequences in terms of diversity gain; the feasibility of these diversity antennas thus warrants study. Preliminary results are presented in Chapter 5.

- *Demonstrate the integration of a diversity antenna with sensor node hardware.*

As a proof of concept, a prototype antenna was integrated with sensor node hardware (Freescale MC13192 kit). Having justified the use of simple diversity techniques within severe environments in Chapter 4, this demonstration illustrates the benefit of using such techniques over traditional omni-directional antennas to mitigate deep fades. The demonstration also illustrates the capacity of wireless sensor nodes to utilize simple diversity techniques without requiring complex hardware or energy intensive computation. This work is presented in Chapter 6.

1.4 Thesis Outline

Chapter 1 served as an introduction to wireless sensor networks and presented a key problem facing static WSN operating within metallic cavities. The remainder of this thesis is organized as follows. Chapter 2 presents the background material necessary for understanding the problem presented and the proposed solutions. Specifically, Chapter 2 describes several common propagation models and statistical tools used in describing the channel (air-interface between the transmitter and receiver) and creating WSN link-budgets. Chapter 3 describes a propagation study performed within a wingless, rotary aircraft, and its key conclusions. Building on the results of Chapter 3, Chapter 4 presents

a study of the diversity gains for simple diversity methods (e.g. polarization, spatial, selection, etc...) within an environment which exhibits small-scale fading that is more severe than predicted by the Rayleigh fading model. Chapter 5 further explores fade mitigation techniques by examining the diversity gain benefit of two antennas intended for use in conjunction with WSN: a passive combining antenna, and a two-element antenna array with an extremely small form factor. Chapter 6 demonstrates the integration of a simple diversity antenna with a wireless sensor node. Finally, Chapter 7 draws conclusions from the previously described research and presents current as well as future courses of study.

1.5 References

- [1] MIT Technology Review, "10 emerging technologies that will change the world," MIT Technology Review, February 2003.
- [2] Pottie, G. and W. Kaiser, "Wireless integrated network sensors," *Comm. ACM*, 43(5):51-58, May 2000.
- [3] Estrin, D., L. Girod, G. Pottie and M. Srivastava, "Instrumenting the world with wireless sensor networks," In *Proc. Int'l Conf. Acoustics, Speech and Signal Processing (ICASSP 2001)*.
- [4] Sensors Magazine, "UCSB Nanofabrication Facility Installs Wireless Monitoring System," *Sensors Magazine*, <http://www.sensormag.com>, May 9, 2006.
- [5] Sensors Magazine, "Web-Enabled Mesh Sensor Network Offers Remote PLC and Process Monitoring," *Sensors Magazine*, <http://www.sensormag.com>, April 26, 2006.
- [6] R. Poor, "Wireless Mesh Networks," *Sensors Magazine*, <http://www.sensormag.com>, February 1, 2003.
- [7] Stankovic, J. and Q. Cao, "Wireless Sensor Networks for In-Home Healthcare: Potential and Challenges," in *High Confidence Medical Device Software and Systems (HCMDSS) Workshop*, Philadelphia, PA, June 2-3, 2005.
- [8] Coleri, S., S. Y. Cheung, and P. Varaiya, "Sensor Networks for Monitoring Traffic," In *Forty-Second Annual Allerton Conference on Communication, Control, and Computing*, Univ. of Illinois, Sept. 2004.

- [9] Fubler, H. and S. Schnauffer, "Vehicular Ad-Hoc Networks: From Vision to Reality and Back," 4th Annual IEEE/IFIP Conference on Wireless on Demand Network Systems and Services (WONS), Obergurgl, Austria, January 2007.
- [10] Akyildiz, I., W. Su, Y. Sankarasubramaniam and E. Cayirci, "Wireless sensor networks: a survey, Computer Networks," Volume 38, Issue 4, 15 March 2002, Pages 393-422.
- [11] Petriu, E. "Sensor-Based Information Appliances," IEEE Instrumentation & Measurement Magazine. December 2000.
- [12] Mainwaring, A., J. Polastre, R. Szewczyk, and D. Culler, "Wireless Sensor Networks for Habitat Monitoring," Proceedings of the 1st ACM International Workshop on Wireless Sensor Networks and Applications, September 28, 2002, Atlanta, Georgia, USA.
- [13] Tolle, G., J. Polastre, R. Szewczyk, and D. Culler, "A Macroscopic in the Redwoods," In Proceedings of the Third ACM Conference on Embedded Networked Sensor Systems (SenSys), 2005.
- [14] Frolik, J. "A case for considering hyper-Rayleigh fading channels," IEEE Trans. Wireless Communications, Vol. No. 6, Issue 4, April 2007.
- [15] Rappaport, T. *Wireless Communications, Principles and Practice*, 2 ed., Prentice Hall, 2002.

CHAPTER 2: SMALL-SCALE PROPAGATION MODELING

Modeling of radio propagation is integral to wireless communication systems since it enables one to predict the power required to close a communication link and to provide reliable communications [1]. Chapter 2 details the small-scale fading models utilized throughout the thesis. Specifically, this chapter will provide qualitative explanations for two common small-scale models (Ricean and Rayleigh), along with their respective mathematical and statistical models. In addition, a relatively new model (hyper-Rayleigh) is presented. Finally, the cumulative distribution function representation of the data, which will be used extensively in analyzing the severity of channel fading, is discussed.

2.1 Propagation Phenomenon

In a given wireless environment there are two modes of signal attenuation: large-scale and small-scale propagation. Large-scale propagation is defined as the variation in signal attenuation as a result of large changes in distance, time, or frequency. For example, large-scale models would predict the signal strength change if the communication link were to increase from 1 km to 2 km. Small-scale propagation, as the name implies, refers to the variations in signal fades as a result of small changes in distance, time, or frequency. The variation in signal strength seen in a moving system over a number of seconds is an example of small-scale propagation effects.

For both modes of signal fading, there are several common models used. Models describing large-scale propagation include Free-Space Propagation (for satellite communication), the Plane-Earth Model, and Median Path Loss [1, 2]. Models that

predict small-scale propagation include Ricean fading, Rayleigh fading [2], and, more recently, hyper-Rayleigh fading [3]. While a good understanding of large-scale propagation is important, the research herein focuses primarily on small-scale fading models. Small-scale propagation models are discussed further in Section 2.2 while large-scale fading is examined in Section 3.2.3.

In general, fading models are either physically or statistically based. A physical model takes into account the exact geometry of the surrounding area to compute estimates of propagation behavior. While this method can be accurate, it is also the most computationally intensive and must be recalculated each time the surrounding area changes or wireless device moves. A statistical model is based on empirical propagation characteristics measured in specific environments. A statistical model is less exact than the physical model in that it cannot calculate the exact signal strength at a given location; specifically, it describes channel behavior in more general terms, such as the expected value and the variance. However, the statistical model does reduce the complexity of propagation calculations while remaining effective in predicting received signal strength, making it the preferred method for link-budget calculations [1].

2.2 Physical Underpinnings of Common Small-Scale Fading Models

Knowing the physical underpinnings of some of the common small-scale fading models is important for an intuitive understanding of the phenomena. This section will describe three basic models: Ricean, Rayleigh, and hyper-Rayleigh. The mathematical and statistical models will be accompanied with qualitative explanations.

2.2.1 Ricean Fading

The Ricean (sometimes termed Rician [1] or Rice [4]) fading model is characterized by a line of sight path (LOS) and many, relatively weak multipath components [1]. The Ricean fading model is often used for modeling mobile radio channels which have a consistent LOS path such as cell phones in view of the tower. Figure 2.1 depicts Ricean fading where TX indicates the transmitter and RX indicates the receiver. The large green arrow depicts the LOS path, and the smaller blue arrows depict the relatively weak multipath components.

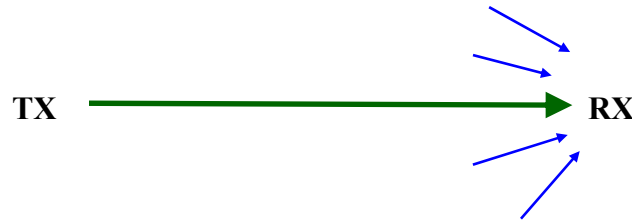


Figure 2.1. Ricean fading scenario

The complex envelope of a radio communication experiencing Ricean fading can be modeled as

$$V_{received} = V_0 + \sum_{i=1}^N V_i e^{j\theta_i} \quad (2.1)$$

where V_0 is the LOS component and the summation is the aggregation of N (which is assumed to be large) randomly reflected paths, each with a complex amplitude V_i , and phase θ_i . In analyzing the Ricean distribution a key factor, entitled the Ricean K -factor, is used. The Ricean K -factor is the ratio of the power in the LOS path to the power in the

reflected paths and is defined as

$$K = \frac{S^2}{\sum_{i=1}^N |V_i|^2} \quad (2.2)$$

where S^2 is equal to $|V_0|^2$, the magnitude of the LOS component squared. The K -factor is usually expressed in dB. An increasing K -factor is indicative of a strong LOS path and a lower probability for deep fades occurring, while a decreasing K -factor indicates a weaker or non-existent LOS path characterized by a higher deep fade probability. The calculation of the Ricean probability density function (PDF) is very involved [1, 4] and well-known and so is given below without derivation.

$$p_R(R) = \frac{R}{\sigma^2} e^{-\frac{(R^2+S^2)}{2\sigma^2}} I_0\left(\frac{RS}{\sigma^2}\right) \quad R \geq 0 \quad (2.3)$$

R represents the envelope amplitude, σ is the standard deviation of the envelope voltage (a variation which is due to the multipath components), and I_0 is the modified Bessel function of the 0th order. I_0 is defined as

$$I_0\left(\frac{RS}{\sigma^2}\right) = \frac{1}{\pi} \int_0^\pi e^{\frac{RS}{\sigma^2} \cos \theta} d\theta \quad (2.4)$$

2.2.2 Rayleigh Fading

In contrast to environments experiencing fading described by the Ricean model, a Rayleigh fading environment is characterized only by many multipath components, each with relatively similar signal strength, and uniformly distributed phase; that is, there is no

LOS path. In short, for Rayleigh fading ($K = 0$ or $K = -\infty \text{ dB}$), communication is conducted entirely as a result of signal reflection and diffraction [2]. This type of fading is often considered a worst-case scenario for mobile communications within urban environments since its defining feature is a lack of the LOS path. Figure 2.2 depicts Rayleigh fading as containing only multipath components, illustrated by the red arrows.



Figure 2.2. Rayleigh fading scenario

The complex envelope of a radio communication experiencing a Rayleigh fading channel can be modeled by

$$V_{received} = \sum_{i=1}^N V_i e^{j\theta_i} \quad (2.5)$$

where each variable maintains the same meaning as in the Ricean case, defined by equation (2.1).

While well known, the Rayleigh distribution is derived so that comparisons can be made. From equation (2.5) it can be seen that $V_{received}$ is a sum of independent and identically distributed (i.i.d.) complex random variables. By virtue of the central limit theorem of statistics, the sum of two or more i.i.d. random variables approaches the Gaussian distribution as the number of random variables (i.e., N) increases [1]. As such,

the PDF of the Rayleigh fading model can be derived from two independent random variables which each represent Gaussian random processes in the x and y dimensions of the Cartesian coordinate system [4]. In this example, x and y represent the two i.i.d. random variables, as before, and σ represents the standard deviation of the envelope amplitude (also known as the rms value of the envelope):

$$p_x(x) = \frac{1}{\sigma\sqrt{2\pi}} e^{\frac{-x^2}{2\sigma^2}} \quad (2.6)$$

$$p_y(y) = \frac{1}{\sigma\sqrt{2\pi}} e^{\frac{-y^2}{2\sigma^2}} \quad (2.7)$$

Since both random variables are independent and identically distributed, the joint distribution can be easily calculated by simply multiplying the two distributions.

$$p_{xy}(x, y) = p_x(x) \cdot p_y(y) = \frac{1}{2\pi\sigma^2} e^{\frac{-(x^2+y^2)}{2\sigma^2}} \quad (2.8)$$

The joint PDF can be simplified by converting the joint distribution from the Cartesian coordinate system to the Polar coordinate system. The amplitude of the complex envelope can be represented by R as defined below.

$$R = \sqrt{x^2 + y^2} \quad (2.9)$$

The phase for each component is represented by θ , and is defined as follows.

$$\theta = \tan^{-1} \frac{y}{x} \quad (2.10)$$

The probability of an event occurring is defined by the area under the PDF bounded by

the range of values the event can take. In a continuum of any range, an uncountable infinite number of values exist with $p_x(x_i)$ (the probability that $x = x_i$, which is generally zero) as one of the infinite values. Hence, for continuous random variables, the meaningful probability is not $x = x_i$ but $x_i < x < x_i + \Delta x$. As a means for defining the joint PDF of R and θ , the probability of observing R and θ in the infinitesimal region bound by $R_i < R \leq R_i + dR$ and $\theta_i < \theta \leq \theta_i + d\theta$ (where both dR and $d\theta \rightarrow 0$) is considered. This probability is simply defined as the joint distribution multiplied by the infinitesimal area.

$$p_{R\theta}(R, \theta) dR d\theta \quad (2.11)$$

In Cartesian coordinates, this probability is also defined by the joint distribution of x and y multiplied by the infinitesimal area of interest. In order to transform the coordinate system from Cartesian to Polar, a change of variables is necessary and is defined as:

$$\iint_D f(x, y) dA = \iint_S f(g(u, v), h(u, v)) \left| \frac{\partial(x, y)}{\partial(u, v)} \right| du dv \quad (2.12)$$

Where $\left| \frac{\partial(x, y)}{\partial(u, v)} \right|$ is the absolute value of the Jacobian, x and y are defined respectively as

$x = g(u, v)$ and $y = h(u, v)$. From this equation, it can be seen that $dA = \left| \frac{\partial(x, y)}{\partial(u, v)} \right| du dv$.

In changing from a Cartesian coordinate system to a Polar coordinate system, x and y are defined as $x = R \cos \theta$ and $y = R \sin \theta$, yielding:

$$dA = dx dy = \left| \frac{\partial(x, y)}{\partial(R, \theta)} \right| dR d\theta = \begin{vmatrix} \frac{\partial x}{\partial R} & \frac{\partial x}{\partial \theta} \\ \frac{\partial y}{\partial R} & \frac{\partial y}{\partial \theta} \end{vmatrix} dR d\theta \quad (2.13)$$

$$\begin{aligned} dx dy &= \begin{vmatrix} \cos \theta & -R \sin \theta \\ \sin \theta & R \cos \theta \end{vmatrix} dR d\theta \\ &= (R \cos^2 \theta - (-R \sin^2 \theta)) dR d\theta \end{aligned} \quad (2.14)$$

$$dx dy = R(\cos^2 \theta + \sin^2 \theta) dR d\theta \quad (2.15)$$

$$dx dy = R dR d\theta \quad (2.16)$$

Using this transformation, the probability of observing R and θ in the area defined by $R dR d\theta$ is:

$$p_{xy}(x, y) R dR d\theta = \frac{1}{2\pi\sigma^2} e^{-\frac{(x^2+y^2)}{2\sigma^2}} R dR d\theta \quad (2.17)$$

By equating the expressions in equations (2.17) and (2.11) and substituting $R^2 = x^2 + y^2$, the joint distribution of R and θ can be solved for as follows.

$$\frac{1}{2\pi\sigma^2} e^{-\frac{(x^2+y^2)}{2\sigma^2}} R dR d\theta = p_{R\theta}(R, \theta) dR d\theta \quad (2.18)$$

$$p_{R\theta}(R, \theta) = \frac{R}{2\pi\sigma^2} e^{-\frac{R^2}{2\sigma^2}} \quad (2.19)$$

Since θ has a uniform distribution, the probability for any given value of θ is:

$$p_{\theta}(\theta) = \begin{cases} \frac{1}{2\pi}, & 0 \leq \theta < 2\pi \\ 0, & \text{elsewhere} \end{cases} \quad (2.20)$$

The joint distribution can be further simplified to a PDF defined only by R , the complex envelope amplitude.

$$p_R(R) = \int_{-\infty}^{\infty} p_{R\theta}(R, \theta) d\theta = \int_0^{2\pi} p_{R\theta}(R, \theta) d\theta \quad (2.21)$$

$$p_R(R) = \int_0^{2\pi} \frac{R}{2\pi\sigma^2} e^{\frac{-R^2}{2\sigma^2}} d\theta = \frac{R}{\sigma^2} e^{\frac{-R^2}{2\sigma^2}} \quad R \geq 0 \quad (2.22)$$

The average power of a signal is a critical parameter in assessing wireless link-quality because it approximates the expected value of the received signal.

The average power (mean square value) of R is found as follows:

$$E[R^2] = \int_{-\infty}^{\infty} R^2 p_R(R) dR = \int_0^{\infty} R^2 \frac{R}{\sigma^2} e^{\frac{-R^2}{2\sigma^2}} dR \quad (2.23)$$

$$u = R^2 \quad (2.24)$$

$$du = 2R dR \quad (2.25)$$

$$dv = \frac{R}{\sigma^2} e^{\frac{-R^2}{2\sigma^2}} dR \quad (2.26)$$

$$v = -e^{\frac{-R^2}{2\sigma^2}} \quad (2.27)$$

Integrating by parts yields:

$$E[R^2] = uv - \int vdu = -R^2 e^{\frac{-R^2}{2\sigma^2}} + \int 2R e^{\frac{-R^2}{2\sigma^2}} dR \quad (2.28)$$

$$E[R^2] = \left[-R^2 e^{\frac{-R^2}{2\sigma^2}} - 2\sigma^2 e^{\frac{-R^2}{2\sigma^2}} \right]_0^\infty \quad (2.29)$$

$$\lim_{R \rightarrow \infty} -R^2 e^{\frac{-R^2}{2\sigma^2}} = 0 \quad (2.30)$$

Equation (2.30) is solved via l'Hopital's rule.

$$E[R^2] = [0 - 0] - [0 - 2\sigma^2] \quad (2.31)$$

$$E[R^2] = 2\sigma^2 \quad (2.32)$$

Equation (2.32) defines the average power as twice the variance of R . This is equivalent to the denominator of equation (2.2) [1]. The median value of equation (2.22) is $R = R_{RMS} = \sqrt{2\sigma^2}$ which infers that 50% of the time there is constructive interference ($R > R_{RMS}$), and destructive interference ($R < R_{RMS}$) for the other 50%. Fifty percent of the samples are expected to be less—and 50% are expected to be greater—than the median, by definition. Use of the median causes all models, regardless of the environment, to intersect at a common point on the cumulative distribution function (discussed later in Section 2.4); this fact proves useful when comparing models. If the mean were to be used, outliers could create significant offsets, making comparisons between models difficult.

2.2.3 Hyper-Rayleigh Fading Regime

Hyper-Rayleigh fading was proposed in [3] to be a fading regime for wireless communication systems operating in metallic cavities such as airframes or buses. As

illustrated in Figure 2.3, hyper-Rayleigh fading is characterized by few strong components (the long green arrows) and very weak scatterers (the relatively short, blue arrows). Methods of modeling this phenomenon will be discussed in the subsequent section. Of the fading regimes discussed, hyper-Rayleigh fading is the most recently described and the least understood. As such, understanding hyper-Rayleigh fading and researching the possible methods of mitigation are the focus of this thesis.

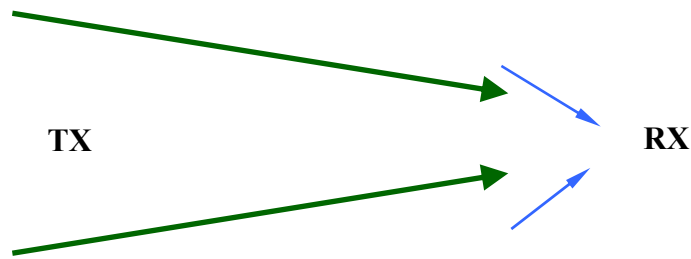


Figure 2.3. Hyper-Rayleigh fading

2.3 Modeling Hyper-Rayleigh Fading

This section describes the development of a hyper-Rayleigh fading model from a recently proposed model known as Two-Wave with Diffuse Power fading (TWDP) [5]. The TWDP model was initially shown to model a variety of fading scenarios including Rayleigh and Ricean. In [3], this model was adapted to also model the hyper-Rayleigh region.

2.3.1 Two-Wave with Diffuse Power Fading

Several propagation models have utilized two strong components for large-scale propagation prediction of LOS communications where a reflection off the Earth provides a second interfering component [3]. Due to the secondary wave reflection off of the

Earth, this two-ray model is also known as the Plane-Earth model [1]. Correspondingly, the TWDP, based on similar geometrics, has been proposed to model small-scale fading [5].

In the TWDP model, the complex baseband voltage seen by the receiver can be written in a similar form to that of equation (2.5). However, for the purpose of modeling hyper-Rayleigh fading, the case under consideration is that in which $V_{received}$ is dominated by two waves with constant amplitude (V_1 and V_2) and random phase (ϕ_1 and ϕ_2). In [5], the two wave components (V_1 and V_2) are referred to as specular components while the remaining contributions to $V_{received}$ are categorized as non-specular or diffuse components. The diffuse components are made up of many waves of random magnitude and phase, the latter being uniformly distributed over $[0, 2\pi)$. The diffuse components are the same as the Rayleigh envelope component in equation (2.5). By adding a dominant component to the diffuse components, the model then applies to a Ricean channel. TWDP is like the Ricean fading model but with two dominant components as is seen in equation (2.33).

$$V_{received} = V_1 e^{j\phi_1} + V_2 e^{j\phi_2} + \sum_{i=3}^N V_i e^{j\phi_i} \quad (2.33)$$

In [5], TWDP uses two factors, K and Δ , to describe the small-scale fading environment and quantify the relative weight of the specular components and their relation to the diffuse component. They are defined as follows:

$$K = \frac{\text{Total Peak Power}}{\text{Average Diffuse Power}} = \frac{V_1^2 + V_2^2}{2\sigma^2} \quad (2.34)$$

$$\Delta = \frac{\text{Peak Specular Power}}{\text{Average Specular Power}} - 1 = \frac{2V_1V_2}{V_1^2 + V_2^2} \quad (2.35)$$

Note that the average diffuse power ($2\sigma^2$) in the denominator of equation (2.34) is the average power found in equation (2.32).

Based on the relative weights between the specular and non-specular components, TWDP can be used to model several different scenarios. As an example, consider when $V_2 = 0$, yielding $\Delta = 0$ and $K = \frac{V_1^2}{2\sigma^2}$; the resulting K corresponds with the Ricean K -factor in equation (2.2). TWDP, it turns out, can be used to not only model Ricean fading, but Rayleigh and hyper-Rayleigh fading as well. Table 2.1 notes the criteria to model certain fading statistics as defined by K and Δ .

Table 2.1. Fading behavior as defined by Δ and K factors.

Fading Behavior	Δ	K	Reference:
Ricean	$\Delta = 0$	$K = \frac{V_1^2}{2\sigma^2}, K > 0$	Durgen [5]
Rayleigh	Anything	$K = 0$	Durgen [5]
Hyper-Rayleigh	$\Delta \approx 1$	$K = \frac{V_1^2 + V_2^2}{2\sigma^2}, K > 0$	Frolik [3]
Two-Ray	$\Delta = 1$	$K = \frac{V_1^2 + V_2^2}{2\sigma^2}, K \rightarrow \infty$	Frolik [3]

In using TWDP to model hyper-Rayleigh fading, a worst-case scenario in which the two waves are completely destructive is considered. Complete destruction can only

occur if the relative phase between the two specular components is π and both components have equal magnitudes, $V_1 = V_2$ ($\Delta = 1$). As such, when $\Delta = 1$ and phase is uniform over $[0, 2\pi)$, equation (2.34) yields the two-ray model which is utilized here for the worst-case scenario for the wireless sensor application under consideration. The PDF for the two-ray model is given in equation (2.36). If the case for hyper-Rayleigh ($V_1 = V_2 = 1$) in equation (2.37) is substituted, the PDF for the hyper-Rayleigh model is given as equation (2.38).

$$p(r) = \frac{2r}{\pi\sqrt{4V_1^2V_2^2 - (V_1^2 + V_2^2 - r^2)^2}} \quad (2.36)$$

$$p(r) = \frac{2r}{\pi\sqrt{4V_1^2V_2^2 - (V_1^2 + V_2^2 - r^2)^2}} \Big|_{V_1=V_2=1} \quad (2.37)$$

$$p(r) = \frac{2r}{\pi\sqrt{4r^2 - r^4}} \quad (2.38)$$

Under the conditions of two random components, we note the resulting distribution is not Rayleigh. This should be expected by virtue of not satisfying the large number criteria for the central limit theorem which leads to equations (2.6) and (2.7).

2.4 Cumulative Distribution Function (CDF)

2.4.1 CDF Theory

To represent the statistical fading models, two approaches are often used: the PDF and the cumulative distribution function (CDF). The PDF of these models describes the probability for a given amplitude of the received signal envelope such as the Rayleigh

distribution in equation (2.5). The CDF is created by integrating the PDF as shown in equation (2.39). The CDF is right continuous and increases monotonically, with $F(-\infty)=0$ and $F(\infty)=1$ [1].

$$F_r(r) = \int_{-\infty}^r p_R(R) dR \quad (2.39)$$

For the Rayleigh PDF, the CDF is:

$$F_r(r) = \int_{-\infty}^r \frac{R}{\sigma^2} e^{\frac{-R^2}{2\sigma^2}} dR = \int_0^r \frac{R}{\sigma^2} e^{\frac{-R^2}{2\sigma^2}} dR \quad (2.40)$$

$$F_r(r) = -e^{\frac{-R^2}{2\sigma^2}} \Big|_0^r = 1 - e^{\frac{-r^2}{2\sigma^2}} \quad r \geq 0 \quad (2.41)$$

For the worst-case ($V_1 = V_2 = 1$) two-ray PDF, the CDF is found as follows:

$$p_r(r) = \frac{2r}{\pi\sqrt{4r^2 - r^4}} \quad r \geq 0 \quad (2.42)$$

$$F_r(r) = \int_{-\infty}^{\infty} p_r(r) dr = \int_0^r \frac{2r}{\pi\sqrt{4r^2 - r^4}} dr \quad (2.43)$$

Using the identity in equation (2.44) and the definitions in (2.45) yield equation (2.46).

$$\int \frac{du}{\sqrt{2au - u^2}} = \text{Cos}^{-1}\left(\frac{a-u}{a}\right) + C \quad \text{for } a > 0 \quad (2.44)$$

$$u = r^2 \quad du = 2rdr \quad a = 2 \quad (2.45)$$

Substituting $u = r^2$ $du = 2rdr$ and $a = 2$ will give $F_r(r)$:

$$F(r)_r = \frac{1}{\pi} \left(\text{Cos}^{-1}\left(\frac{2-r^2}{2}\right) + C \right) \Big|_0^r \quad (2.46)$$

$$F_r(r) = \frac{1}{\pi} \left[\text{Cos}^{-1} \left(\frac{2-r^2}{2} \right) + C - \text{Cos}^{-1} \left(\frac{2-0}{2} \right) - C \right] \quad (2.47)$$

$$F_r(r) = \frac{1}{\pi} \left[\text{Cos}^{-1} \left(\frac{2-r^2}{2} \right) \right] \quad (2.48)$$

$$\text{Identity: } \text{Cos}^{-1}(x) = \pi - \text{Cos}^{-1}(-x) \quad (2.49)$$

This gives the following as the definition for the two-ray CDF:

$$F_r(r) = 1 - \frac{1}{\pi} \text{Cos}^{-1} \left(\frac{r^2-2}{2} \right) \quad r \geq 0 \quad (2.50)$$

2.4.2 Modeling and Empirical Use of the CDF

The CDF is incredibly useful in characterizing the fading wireless environments and therefore in developing link budgets. For a given wireless environment, the CDF of empirical data is found by first normalizing by the median received signal strength, which represents the large-scale fading. The remaining normalized data represents the small-scale fading. The CDF is created by normalizing the data with respect to the large-scale path loss and plotting it relative to the probability that it occurs. Figure 2.4 illustrates the Rayleigh and two-ray CDF, equations (2.41) and (2.50), respectively. The vertical line at the $x = 0$ tick mark illustrates the fading probability for the ideal case in which no fading occurs. This cumulative fading probability is a step function in which a fade greater than 0 dB occurs with 0% probability while a 0 dB fade occurs 100% of the time. These curves will serve as a basis for categorizing our fading data.

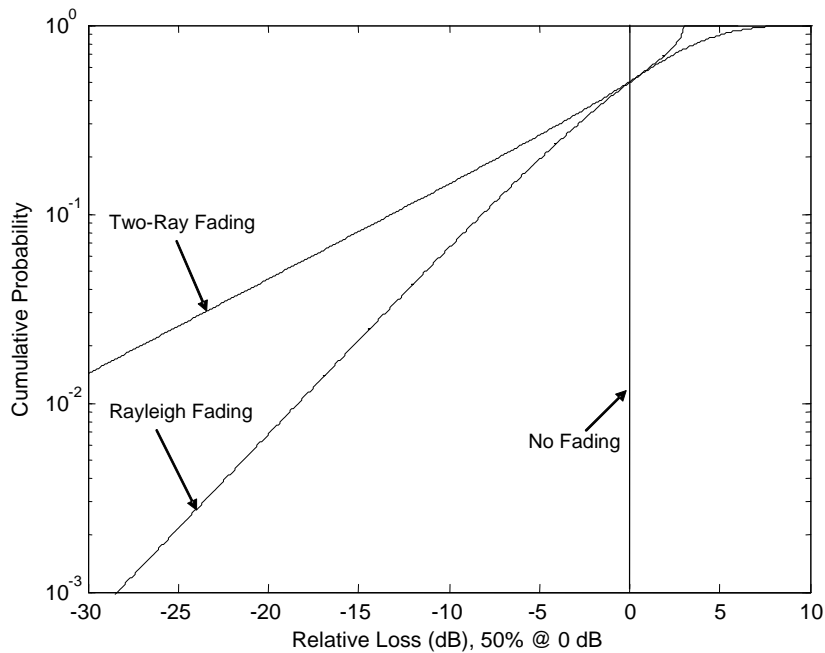


Figure 2.4. CDF of Rayleigh and two-ray fading

Figure 2.5 is a CDF which illustrates the cumulative probability of fades predicted by different models. From the figure, it can be seen that the respective cumulative probability decreases as fade depth (Loss) increases. As the models rotate clockwise they predict an increasingly severe environment. The region between Rayleigh fading and no fading is less severe and is captured by the Ricean model which begins to model a Rayleigh environment as $K \rightarrow 0$, and as $K \rightarrow \infty$, the Ricean model becomes comprised of only the dominant path as in the no fading case. The region above the Rayleigh curve is the domain of hyper-Rayleigh fading. From Figure 2.5, it is readily seen that a given fade has a higher probability of occurrence when considering the two-ray model than the Rayleigh model. For example, a 20 dB fade has an approximate cumulative probability of 0.7% within a Rayleigh environment whereas within a two-ray environment the

cumulative probability is 5%.

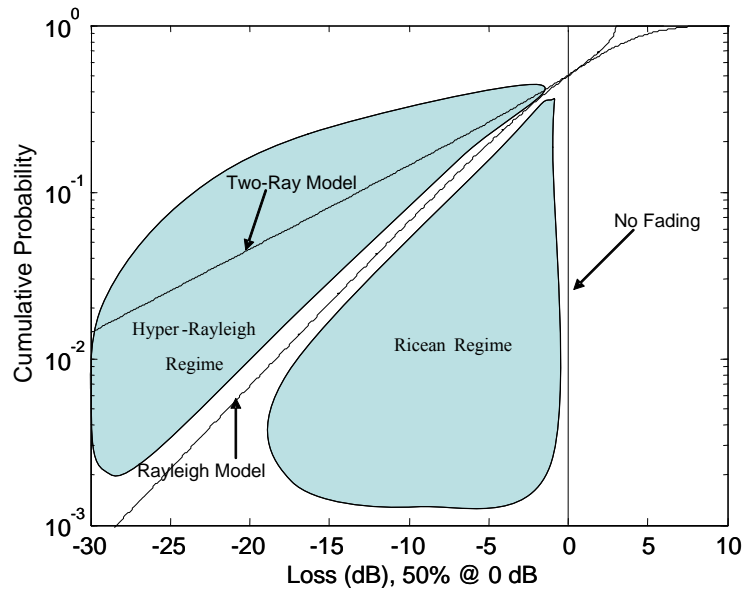


Figure 2.5. CDFs of the fading models and hyper-Rayleigh fading

To illustrate the use of a CDF like that given in Figure 2.5, consider the scenario in which a wireless communication system requires 99% reliability at the edge of coverage and utilizes radios sensitive to -100 dBm. Assuming that the system is operating within a Rayleigh environment, the CDF can be used to find the fade margin needed to guarantee 99% system reliability. The fade margin can be found by locating the fade on the Rayleigh curve that has 1% cumulative probability. In this case, the fade margin is approximately 18 dB which means that, at the edge of coverage, the median received signal would need to be -82 dBm or greater. In other words, a signal with a median value of -82 dBm is the lowest the system can receive and still retain 99% system reliability. If the environment exhibited two-ray fading, the fade margin would need to

increase to approximately 35 dB, leaving only -65 dBm as the minimum median received signal strength for 99% system reliability.

2.5 Conclusions

In this chapter, three models were presented for modeling small scale fading: two very common models, Ricean and Rayleigh, and a third model, hyper-Rayleigh. Ricean fading is defined by a LOS component and small, relatively weaker multipath components. Rayleigh, unlike Ricean, does not have a LOS component but has multipath components that are similar in strength and uniformly distributed in phase. Rayleigh communication is exclusively conducted via reflections and diffraction of the signal. Hyper-Rayleigh fading occurs when two rays of similar magnitude add with random phase, which is uniformly distributed over $[0, 2\pi)$. The TWDP model has been introduced as an all encompassing model which includes Ricean and Rayleigh fading and has been adapted to model the hyper-Rayleigh region as well. Finally, the cumulative distribution function, which illustrates the cumulative probability of a fade occurring relative to the median receive value, was introduced as a tool for determining how best to characterize the channel. The CDF will later be used to characterize fading channels within aircraft and will also be used to quantify how well certain diversity techniques mitigate fades.

In Chapter 3 an analysis of empirical data collected from in-aircraft wireless propagation tests is presented. The analysis shows that fading is prevalent in all three fading regimes with a key result of the investigation being that small-scale frequency-selective often exceeds severity predicted by current worst case fading models (i.e.

Rayleigh).

2.6 References

- [1] Haykin, S. and M. Moher, *Modern Wireless Communications*, Pearson Education, Inc. 2005.
- [2] Rappaport, T. *Wireless Communications, Principles and Practice*, 2 ed., Prentice Hall, 2002.
- [3] Frolik, J. "A case for considering hyper-Rayleigh fading channels," IEEE Trans. Wireless Communications, Vol. No. 6, Issue 4, April 2007.
- [4] Lathi, B.P. *Modern Digital and Analog Communication Systems*, 3 ed., Oxford University Press, 1998.
- [5] Durgin, G., T. Rappaport and D. de Wolf, "New analytical models and probability density functions for fading in wireless communications," IEEE Trans. Communications, Vol. 50, No. 6, June 2002.

CHAPTER 3: PROPAGATION CHARACTERIZATION FOR IN-AIRCRAFT WIRELESS SENSOR SYSTEMS

3.1 Foreword

This chapter presents a propagation study of the environment within a wingless, rotary aircraft. Propagation characterization is an important measure in the development of wireless sensor systems because it supplies a useful metric for designers to use in designing link-budgets. Metallic cavities are of particular interest because previous work conducted within a bus and on a passenger jet have indicated that their respective propagation characteristics exhibit fading more severe than predicted by present worst-case fading models for mobile systems. This work presented is in an effort to extend research already conducted within other metallic cavity environments. Sections 3.2 through 3.5 are presented as submitted (November 2006) for review for publication in IEEE Transactions on Aerospace and Electronic Systems.

3.2 Propagation Characterization for in-Aircraft Wireless Sensor Systems

3.2.1 Abstract

Wireless sensors will enable a new generation of aircraft support systems. However, metallic airframes can produce severe propagation effects as illustrated by the measurements presented herein. The key finding is that it is not uncommon for frequency-selective fading statistics to be more severe than predicted by present worst-case models.

3.2.2 Introduction

In recent years, the diverse potential applications for wireless sensor networks (WSN) have been touted by researchers and the general press. In particular, WSN are seen as an enabling technology for the distributed monitoring of industrial, military and natural environments with unprecedented spatial and temporal resolution. In comparison to cellular communication systems, WSN are unique due to their deployment location (e.g., near-ground, underground, at air/water boundaries or embedded in composite structures) and typical static nature; as such, current propagation and fading models for mobile systems may not necessarily be applicable.

WSN in particular show promise for aircraft support systems that provide non-essential but highly desirable information. For example, a system of distributed accelerometers and/or strain gauges could be valuable for conditional maintenance. However, commercial aircraft already have 2000 to 5000 pounds of wiring; thus, the added weight of a *wired* sensor network is not desirable. Furthermore, wiring is vulnerable to vibration, hardening, and breakage. Wiring insulation degrades as a result of exposure to moisture, temperature cycling, fungus, and aviation chemicals, leading to potential shorting or intermittent performance [1]. Faults of this type are extremely difficult to localize, and work is being done to develop sensing systems to find such insulation problems [2]. In addition, wiring is also a primary entry point for electromagnetic effects (e.g., lightning) that can disrupt or damage aircraft electrical/electronic systems. Hence, a distributed WSN offers advantages in terms of

reduced weight and complexity. To date, FCC Part 15 wireless systems are being used for smoke detection [3], video security [4], and for control of emergency lighting [5].

Airframes, however, are far from being a free space environment due to reflections occurring from their enclosed, metallic structure. This provides motivation to better understand the propagation effects that would be experienced in a wireless sensor deployment. The work presented herein builds upon earlier results in which data was collected within two common commercial aircraft in the 2.4 GHz (Industrial, Medical and Scientific) ISM band [6]. That work presented the variability in signal strength (in dB) observed across the band for 18 locations measured on a 747-400 and 16 records aboard a MD-90. The data also indicated that for some locations the fading severity exceeded that predicted using the Rayleigh channel assumption (typically considered worst-case scenario in wireless systems analysis). This class of channels was referred to as exhibiting *hyper-Rayleigh* behavior. Those results motivated a theoretical development of a new worst-case, two-ray fading model in [7] which is a special case of the two-wave, diffuse power (TWDP) developed in [8]. The two-ray model was used in [9] to ascertain the effectiveness of employing diversity methods in such hyper-Rayleigh environments.

The work herein presents the results of a more extensive measurement campaign aboard a large, non-fixed wing aircraft. While the 2.4 GHz band has garnered interest for WSN applications particularly due to the recently introduced IEEE 802.15.4/ZigBee hardware, also considered herein are the 433 MHz, 915 MHz and 5.1 GHz ISM bands. The measurements yield both characterization of large- and small-scale propagation for

this environment. In particular, the major contribution of this work is the empirical data which demonstrate that hyper-Rayleigh small-scale fading is more than a theoretical construct. The paper is organized as follows. In Section 3.3 we present the environments characterized, the test methodology and analysis methods. In Section 3.4, we discuss the empirical data and analysis results. Section 3.5 concludes with the key results and directions for future work.

3.3 Test Methodology

3.3.1 Environment Characterized

For this work, six primary monitoring locations were considered within a large, non-fixed wing aircraft (Figure 3.1 and Table 3.1). The motivating assumption was that the wireless system would be configured in a single-hop, star network with the hub located in the equipment bay (positioned behind the cockpit – location X in Figure 3.1). In each location, antennas were mounted on the structure, thereby mimicking deployment of wireless data and/or sensor nodes. This mounting condition is a unique constraint for this application space (as opposed to handheld mobile or wireless laptop applications) in that installation is in direct proximity to a large reflecting surface. As such, unique propagation effects should be foreseen. For the presented test scenarios, the assumption is that the sensors would be statically deployed. For testing, the cavities were also static (i.e., no moving passengers).

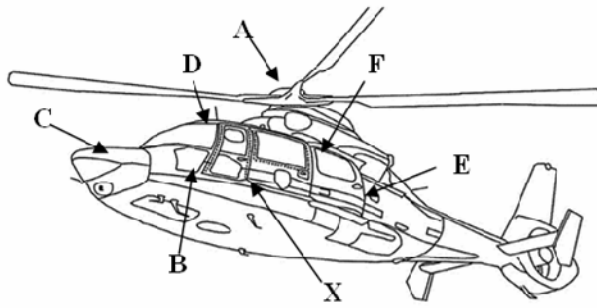


Figure 3.1. Test locations within transport helicopter

Table 3.1. Test location features

Location (Reference in Fig. 1)	Distance from Equipment Bay (X)	Location Features
Rotating Frame (A)	~4.5 m	External on top of rotating beanie
Pilot Floor (B)	~2.0 m	Underneath pilots seat, left side
Cockpit Display (C)	~3.0 m	Behind cockpit display, inside nose
Cockpit Ceiling (D)	~3.5 m	Ceiling above right side seat
Passenger Bulkhead (E)	~6.0 m	Rear of passenger compartment, adjacent to tail bulkhead and above the rear hatch
Passenger Bay Ceiling (F)	~3.5 m	Ceiling, Center of passenger bay

To measure the propagation loss between each location (Locations A-E) and the hub (Location X), a calibrated setup using a vector network analyzer (VNA) was employed (Figure 3.2). A cable connected port 1 of the VNA (a four port Agilent 50711B) with a dipole transmit (TX) antenna. This antenna was mounted within the equipment bay (Location X – the hub) on a magnetic base. Ports 2-4 were similarly attached to receive (RX) antennas that were placed in one of the six test locations (e.g.,

‘C’ as illustrated in Figure 3.2). A similar test configuration has been utilized for characterizing a variety of wireless environments including those within buildings [10].

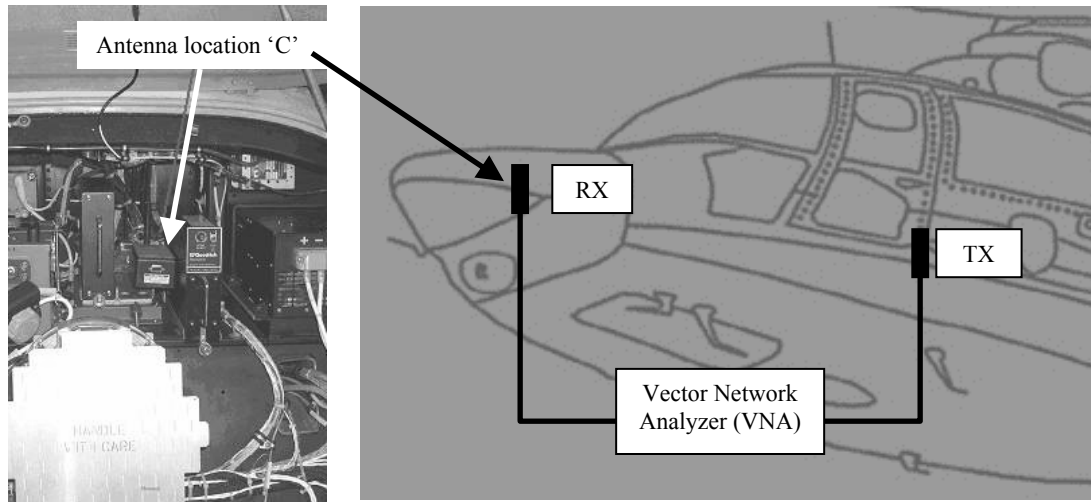


Figure 3.2. Measurement setup for test location ‘C’

Each data set consisted of a frequency sweep conducted over one of four ISM bands (per Table 3.2). We justify the limited sweep ranges by considering the motivation for having propagation models in the first place. For example, an appropriate fading model enables one to analyze the effectiveness of diversity methods to mitigate fading. One such method is to utilize frequency diversity, in which the channel of choice is constrained to fall exclusively within the allocated bandwidth (i.e., per Table 3.2).

Table 3.2. ISM bands characterized

Band	Start Frequency	Stop Frequency	Bandwidth
433 MHz	430 MHz	435 MHz	5 MHz
915 MHz	902 MHz	928 MHz	26 MHz
2.4 GHz	2400 MHz	2480 MHz	80 MHz
5 GHz	5150 MHz	5350	200 MHz

In this work, each frequency sweep presented consists of ~300 data points (i.e., magnitude of loss in dB versus frequency in Hertz). An example data set is provided in Figure 3.3.

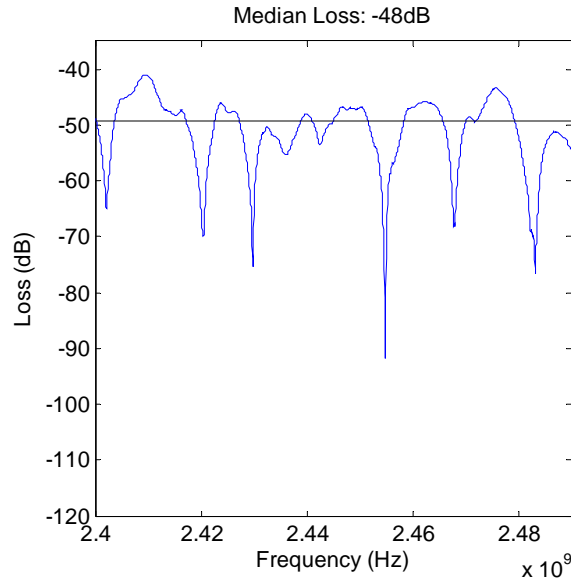


Figure 3.3. Example frequency response (dB vs. Hz) taken at the passenger bulkhead (position ‘E’)

To characterize the link between the test locations (A-E) and the hub (X), 20 test positions were considered. These multiple positions were selected to understand the effects as a result of small- ($< \lambda$ – less than one wavelength) and medium-scale ($> 2\lambda$) spatial displacements within the environment. In addition the transmit antenna at each test position was oriented to be either horizontally or vertically polarized. The purpose of measuring these two responses was to collect data on the effectiveness of employing polarization diversity to mitigate fades. In short, for each location ~40 data sets were conducted (these are enumerated in Appendix A).

3.3.2 Analysis Methods

There are two approaches to modeling a communication environment: physically and statistically. The physical method involves the development of, for example, a ray-tracing model to determine the path-loss for each link. This approach, however, requires extensive computation, as well as detailed understanding not only of the environment's geometry and materials, but also the specific orientation of wireless hardware (i.e., antennas). As such, results may be suitable to understanding large-scale propagation effects for relatively simplistic environments. Clearly, an airframe does not meet this constraint and, accordingly, we consider the alternative statistical methods for our propagation characterization.

3.3.3 Large-scale analysis

Large-scale propagation refers to the change in signal strength as a result of large changes in distance. In our application for example, large-scale analysis would be used to understand the difference in signal strength between what is observed at two different locations within the structure. From the wireless application spaces of satellite systems to cellular communications, many large-scale models have been utilized to better understand these communication links. Most, however, assume the environments to be generally homogeneous. One such empirically-based model is the well-known log-normal shadow model [11] illustrated in (3.1). In this model, $L_p(r)$ is the modeled loss in dB at distance r . $L_p(r_0)$ represents the measured path-loss at the reference distance r_0 , and n is the path-loss exponent which ranges from 2 (free space) to 5 (dense urban

areas). To account for variability in the environment, the model also includes a random component X_σ , which is a zero-mean, Gaussian random variable with standard deviation σ dB. In short, (3.1) is a parametric model in n and σ .

$$L_p(r) dB = L_p(r_0) dB - 10n \text{Log}(r/r_0) + X_\sigma \quad (3.1)$$

Our application has an undisputedly non-homogeneous environment due to the aircraft's numerous partitions, seats, and equipment racks. To account for such attenuating barriers in buildings, for example, (3.1) has been extended to include additional fixed losses caused by floors and walls to create an indoor path loss model. As illustrated in (3.2), fixed loss wall attenuation factors (WAF ; in dB) and floor attenuation factors (FAF) are added to account for these structures.

$$L_p(r) dB = L_p(r_0) dB - 10n \text{Log}(r/r_0) + \sum_{p=1}^P WAF(p) + \sum_{q=1}^Q FAF(q) + X_\sigma \quad (3.2)$$

Variables p and q are the number of walls and floors, respectively. The indoor path-loss model however, does not account for variable attenuation due to incidence angle and thus should only be considered for a rough estimate. In our application, the theoretical loss through metallic barriers is infinite but, due to coupling and diffraction, communication is possible between cavities in an airframe. However, measuring or calculating a WAF and FAF for our space as a means of capturing this phenomenon is intractable since the loss posed by the barrier depends not only upon the shape of the structure but also upon the distance separating it from the signal source. In short, this problem renders (3.2) impractical for our application.

As such, for our work we characterize the large-scale propagation effects using the median path loss measured at a particular location. We view our approach as being novel in that we are not collecting a series of measurements made over time, but in that the data is collected over frequency, polarization, and small increments of space (note that the environment considered is static so there is no temporal component to consider). For example, for the data presented in Figure 3.3, the median path loss across the frequency band is -48.0 dB (the horizontal line appearing in the graph).

One notes that as a function of frequency there are several nulls in the response. These nulls are due to small-scale effects to be discussed in the subsequent section. For our large-scale characterization we utilize this sweep (measurements of signal power with respect to frequency) to calculate the median loss. Such a median is calculated for each of the ~40 data sets measured at each location and frequency band. The average of these median values was calculated, along with the standard deviation from it. We view our methodology to be a specialized case of (3.1) and (3.2) in which the median value captures all but the standard deviation. As such we may express our resulting model for the i^{th} location as

$$L_{p,i} \text{ dB} = \text{median}(L_{p,i} \text{ dB}) + X_{\sigma,i} \quad (3.3)$$

We present and discuss our large-scale analysis results in Section 3.4.1.

3.3.4 Small-scale analysis

Our choice of utilizing the median response rather than the mean for our large-scale analysis stems from the approach utilized for characterizing small-scale effects.

Small-scale fading is characterized by large changes in loss that occur over small increments of time, space or frequency. Small-scale fading is also referred to as multipath fading since the phenomenon is caused by the signal traveling multiple paths and the received components adding destructively.

For example, it is well known that for channels where there exist a large number of multipath components, each of random amplitude and phase, the summation creates a complex envelope. There, by virtue of the central limit theorem, the real and imaginary components tend to a Gaussian distribution; it can thus be shown that the magnitude of the envelope is Rayleigh distributed and the phase component is uniformly distributed [11]. For mobile systems, where it can generally be assumed that there is a large number of scatterers, the Rayleigh fading channel is a normal requisite condition for performance analyses. In Figure 3.4, the cumulative distribution functions, *CDF*, for a Rayleigh fading channel is presented. The Rayleigh model has been normalized by the median fade value so that the curve passes through a (0dB - median, 50% cumulative probability) crossover point. Using the median as our metric ensures that all curves path through the crossover.

The *CDF* curve enables system designers to set link margins based on an allowable outage probability. For comparison, the no-fading case (constant signal strength over small-scales in time, frequency and position), is provided and seen to be a unit step occurring at 0 dB. To use the case presented in Figure 3.4 as an example, achieving an outage probability of less than 1 % requires that a system operating in a Rayleigh environment be designed to have an ~18 dB fade margin (relative to the median value).

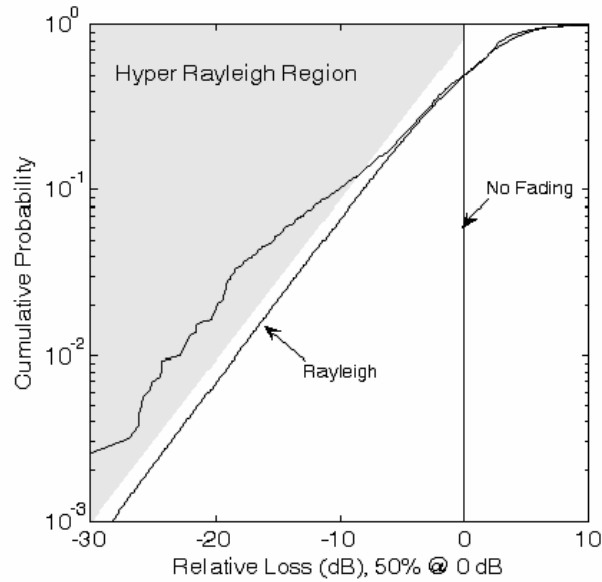


Figure 3.4. Utilization of CDF curve to categorize small-scale fading. The response presented in Figure 3.3 is seen to exhibit hyper-Rayleigh fading statistics.

In related work [7], we presented a theoretical development and empirical results demonstrating the existence of what we refer to as hyper-Rayleigh fading or fading more severe than Rayleigh. The hyper-Rayleigh region is illustrated on the *CDF* curve of Figure 3.4. As noted in Figure 3.3, the median loss value of that data is -48 dB. Using the median as a reference, the probability of fades and constructive interference can be ascertained. These probabilities can thus be used to develop a *CDF* for this data set, also plotted on Figure 3.4. As can be seen, this data is an example of hyper-Rayleigh frequency-selective fading; the fade statistics (e.g., for 20 or 30 dB fades) are more severe than predicted by the Rayleigh fading model.

In contrast, should there be a single strong line of sight component along with

weaker multipath components, the probability of deep fades will be reduced and the resulting *CDF* plot will lie below the Rayleigh curve. This class of fading is referred to as Ricean fading [11] and has long been studied (along with Rayleigh) for wireless communication systems.

The benefit of utilizing an appropriate fading model for energy-limited WSN applications is that it allows the designer to minimize transmission power and extend the system life. Furthermore, as noted, utilizing appropriate fading models enables the performance of fade-mitigating diversity methods to be analyzed. To date, mitigation of hyper-Rayleigh fading remains an area of ongoing work [9]. Our objective herein is to illustrate that such fading is not a theoretical curiosity but rather a prevalent phenomenon in locations such as airframe environments, particularly the environment discussed in Section 3.3.1.

3.4 Results and Discussion

3.4.1 Large-scale Results

The results of our large-scale analysis for the six locations in the studied airframe are presented in Table 3.3. From the free space path loss equation (3.4), the path loss is expected to increase with frequency (i.e., as wavelength λ decreases).

$$L_p(r) = \left(\frac{4\pi r}{\lambda} \right)^2 \quad (3.4)$$

As such, relative to the loss at 433 MHz, we expect an additional ~ 6.5 dB loss at 915 MHz, ~ 14.8 dB at 2.4 GHz and ~ 21.2 dB at 5 GHz. We see that this is the case for

all locations except ‘B’ (under the pilot’s seat). Since shielding becomes less effective with shorter wavelengths (i.e., increasing frequency), our data illustrates a partial shielding condition for this location. Variability between the measured positions at each location resulted in standard deviations in the range of 1.7 to 4.1 dB. While the 433 MHz band had the lowest loss (with the aforementioned exception of location ‘B’), no particular band was found to be more consistent (lower standard deviation) in its measurements. Our worst-case locations were located in the rotating frame (A) and the cockpit display (C) where the path loss ranged between 60 and 70 dB at 2.4 GHz.

Table 3.3. Summary of path loss data

Band	Location	Median Loss (dB)	s.d. (dB)	Location	Median Loss (dB)	s.d. (dB)
433 MHz	A	-36.5	3.2	D	-39.0	3.2
	B	-44.2	4.2	E	-34.7	3.6
	C	-59.6	5.5	F	-31.0	4.6
915 MHz	A	-40.9	4.1	D	-42.4	2.8
	B	-45.5	3.1	E	-38.4	2.7
	C	-66.0	2.8	F	-39.0	2.7
2.4 GHz	A	-62.8	2.3	D	-48.1	2.3
	B	-49.1	3.0	E	-45.2	1.7
	C	-70.1	3.3	F	-44.7	2.4
5 GHz	A	-70.9	3.3	D	-57.0	3.5
	B	-57.7	2.6	E	-53.5	2.0
	C	-77.3	2.6	F	-52.4	2.1

Even at 70.1 ± 3.3 dB, we would not expect link issues related to large-scale propagation effects since typical wireless sensors systems can handle losses on the order of 90 dB. However, frequency selective fading can easily contain fades on the order of 30 dB, especially in the higher frequency bands. This, coupled with the median path-loss, is enough to prevent communication, and provides motivation to study the statistics

associated with such small-scale path-loss. Our results for the studied environment are discussed in the following section.

3.4.2 Small-scale Results

Using our data sets, we categorized our records as being Ricean, Rayleigh or hyper-Rayleigh. Rayleigh fading is a theoretical construct, thus for our purposes we defined criteria (Table 3.4) to indicate that the fading statistics were ‘Rayleigh-like’ (as opposed to exactly Rayleigh).

Table 3.4. Fading classification criteria

Classification	Criteria
Ricean	$P(20\text{ dB fade}) \leq 0.1\%$
Rayleigh	$P(20\text{ dB fade}) > 0.1\%$ and $\{ P(27.5\text{ dB fade}) \leq 0.15\%$ or $P(22.5\text{ dB fade}) \leq 0.52\%$ or $P(25\text{ dB fade}) \leq 0.52\% \}$
Hyper-Rayleigh	Otherwise or $P(30\text{ dB fade}) \geq 0.1\%$

Our resulting classification for measurements conducted in the 915 MHz, 2.4 GHz and 5 GHz ISM bands are presented in Table 3.5, Table 3.6, and Table 3.7, respectively. Fading across the 433 MHz band was minimal in that over 90% records were classified as Ricean. Even in these frequency bands, however, deep fades occurred and frequency-selective hyper-Rayleigh fading was noted in up to 8% of the records for some locations.

While the 433 MHz band is most benign in terms of fading, there is motivation not to deploy systems utilizing this frequency band. Foremost is that, due to the longer wavelengths, antennas are physically larger than for the higher bands and, as illustrated, the band is more susceptible to partial shielding effects. In addition, only 5 MHz of bandwidth is available in this band thereby limiting the scope of a potential sensor deployment. Among the higher three bands, all were found to have a significant number (> 20 %) of cases exhibiting hyper-Rayleigh fading.

Table 3.5. Classification of fading measurements conducted for the 915 MHz ISM band

Location	No. of Measurements	Ricean	Rayleigh	Hyper-Rayleigh
A	31	74%	7%	19%
B	31	71%	3%	26%
C	31	71%	19%	10%
D	31	77%	0%	23%
E	31	81%	3%	16%
F	31	71%	16%	13%

Table 3.6. Classification of fading measurements conducted for the 2.4 GHz ISM band

Location	No. of Measurements	Ricean	Rayleigh	Hyper-Rayleigh
A	40	55%	25%	20%
B	40	67.5%	10%	22.5%
C	39	33%	41%	27%
D	42	48%	26%	26%
E	42	26%	45%	29%
F	42	43%	36%	21%

Table 3.7. Classification of fading measurements conducted for the 5 GHz ISM band

Location	No. of Measurements	Ricean	Rayleigh	Hyper-Rayleigh
A	40	27.5%	50%	22.5%
B	40	25%	47.5%	27.5%
C	40	0%	62.5%	37.5%
D	40	32.5%	50%	12.5%
E	40	22.5%	65%	12.5%
F	40	22.5%	55%	22.5%

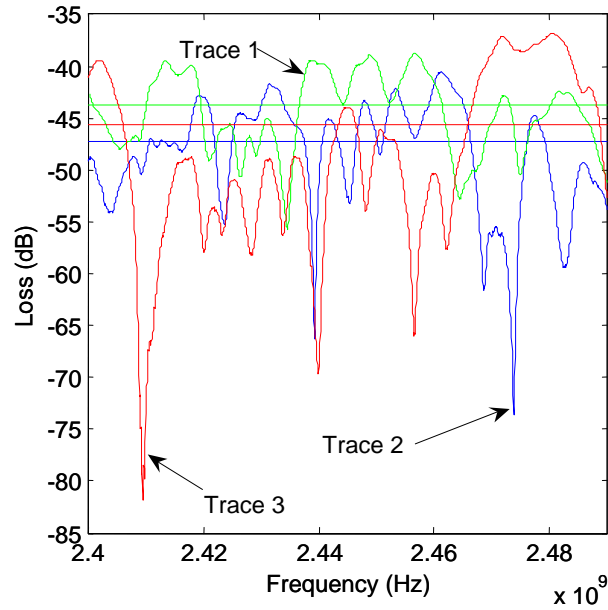


Figure 3.5. Frequency-selective fading within passenger bulkhead exhibiting (*Trace 1*) Ricean, (*Trace 2*) Rayleigh, and (*Trace 3*) hyper-Rayleigh characteristics.

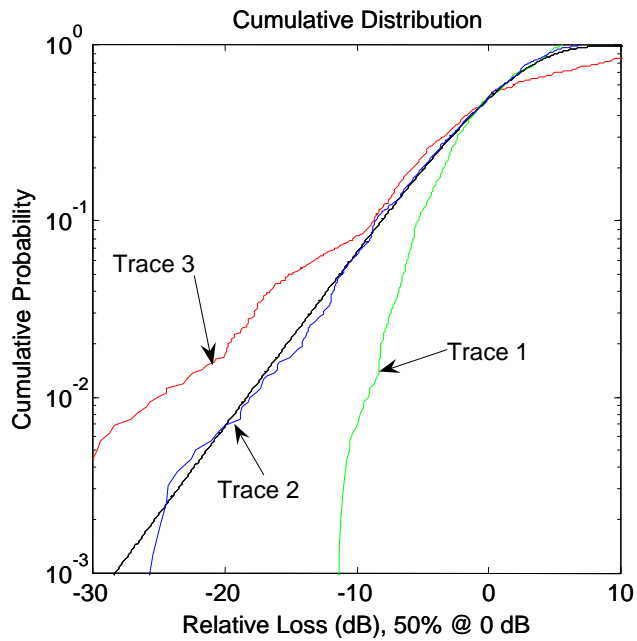


Figure 3.6. *CDF* curves for frequency selective fading measurements depicted in Figure 3.5

To illustrate the small-scale data variability within each location, Figure 3.5 presents three measurements made with the receive antenna fixed in the passenger bulkhead (Location E) and the transmitting antenna moved to three different positions in the equipment bay (Location X). While these three records exhibit similar large-scale behavior in that their median losses are -43.8 dB (*Trace 1*), -45.6 dB (*Trace 3*), and -47.2 dB (*Trace 2*), their fading statistics are significantly different. *Trace 1* is seen to exhibit benign fading and we see that the *CDF* in Figure 3.6 reflects this Ricean behavior. In contrast, *Trace 3* exhibits > 30 dB fades and statistics overall more severe than predicted by the Rayleigh fading model (which is closely matched by *Trace 2*).

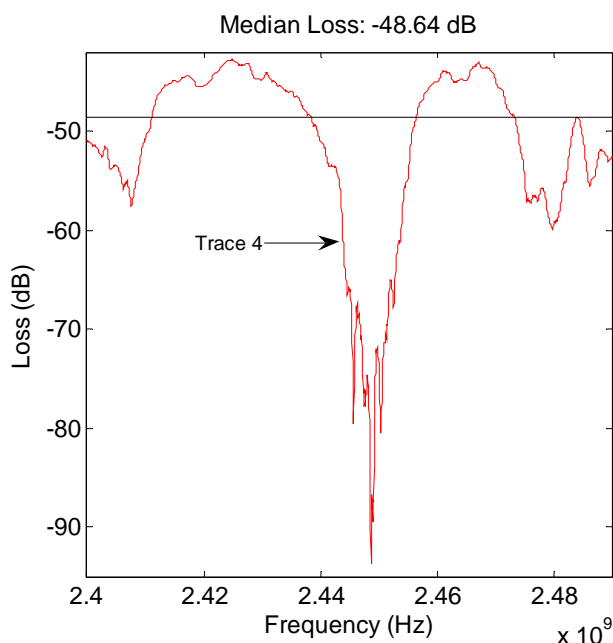


Figure 3.7. Example measurement (location ‘D’) exhibiting severe frequency-selective fading

As noted, a two-ray model was proposed in [7] as a worst-case, hyper-Rayleigh scenario for frequency-selective fading in cavity structures. Figure 3.7 and Figure 3.8 present a data record (*Trace 4* – from location ‘D’) showing that fading with this severity is indeed possible; continued work in mitigating such fades is thereby further motivated.

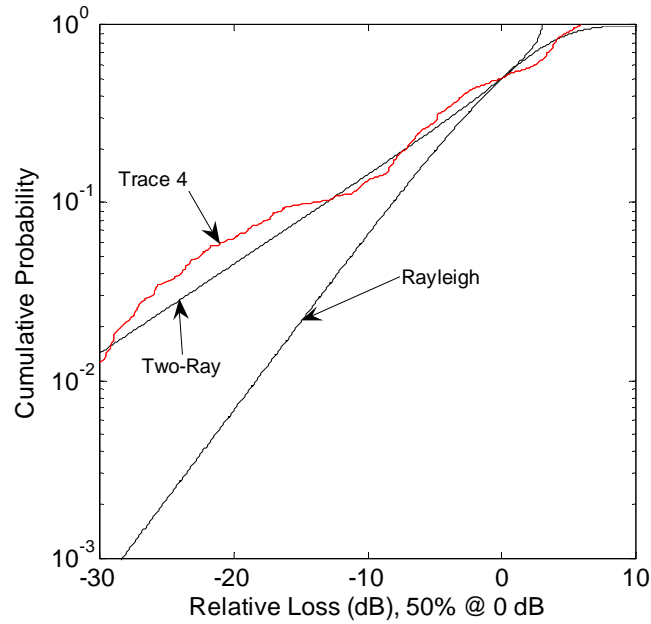


Figure 3.8. CDF of Figure 3.7 exhibiting two-ray fading statistics

3.5 Conclusions

Herein we present empirical large- and small-scale propagation data collected at six locations within a large aircraft with unfixed wings. Given the complex environment, we develop a stochastic large-scale model in which the median loss is characterized along with a random component. We categorize small-scale fading by the frequency-selective fading statistics noted in frequency sweeps. For the test locations considered, large-scale path loss would indicate that reliable communications is readily achievable. However,

due to the cavity structure, multipath is all but guaranteed and small-scale fading is therefore of concern. The key result of this investigation is that small-scale frequency-selective fading often exceeds the severity predicted by Rayleigh fading models. As such, system designers should employ diversity techniques wherever possible to mitigate these fades. While diversity techniques (e.g., antenna or spatial diversity) methods have been well studied, their performance has been quantified assuming a Rayleigh-fading environment. As such, work remains to consider the performance of such methods for channels that exhibit hyper-Rayleigh characteristics.

3.6 References

- [1] Joint Council on Aging Aircraft (JCAA), "A national strategy for aging aircraft," July 2004.
- [2] Waddoups, B., C. Furse and M. Schmidt, "Analysis of reflectometry for detection of chafed aircraft wiring insulation," Fifth Joint NASA/FAA/DoD Conference on Aging Aircraft, Orlando, FL 2001.
- [3] Securaplane Technologies, Inc., "Wireless Smoke Detection," online: <http://www.securaplane.com/smoke2.html>, Securaplane Technologies Inc. November 12, 2006.
- [4] St. John, E. "Operational Issues Wireless Overview," presented at the World Airline Entertainment Association Single Focus Workshop (WAEA SFW), November 19-20, 2002, Washington DC.
- [5] Securaplane Technologies, Inc., Press Release, "Securaplane Technologies Awarded Boeing 787 Contract for Wireless emergency lighting, December 21, 2004, online: <http://www.securaplane.com/releases/pr0095.html> (21Nov06)
- [6] Fitzhugh, C., J. Frolik, J. Covell, R. Ketcham, and T. Meyer, "2.4 GHz multipath environments in airframes," 2005 Wireless and Microwave Technology Conference (WAMICON 2005), Clearwater, FL, April 7-8, 2005.
- [7] Frolik, J. "A case for considering hyper-Rayleigh fading channels," IEEE Trans. Wireless Communications, Vol. No. 6, Issue 4, April 2007.
- [8] Durgin, G., T. Rappaport and D. de Wolf, "New analytical models and probability density functions for fading in wireless communications," IEEE Trans. Communications, Vol. 50, No. 6, June 2002.

- [9] Ketcham, R., J. Frolik, B. Zivanovic, S. Melias, and T. Weller, "Effectiveness of simple diversity methods in mitigating hyper-Rayleigh fading environments," 2006 IEEE Wireless and Microwave Conference, Clearwater FL, December 4-5.
- [10] Chong, C-C. and S. Yong, "A generic statistical-based UWB channel model for high-rise apartments," IEEE Trans. Ant. and Prop., Vol. 53, No. 8, August 2005, pp. 2389-99.
- [11] Rappaport, T. *Wireless Communications, Principles and Practice*, 2 ed., Prentice Hall, 2002.

CHAPTER 4: COMPACT AND SIMPLE DIVERSITY METHODS FOR MITIGATING SEVERE FADING

4.1 Foreword

This chapter builds on the conclusions of Chapter 3; that is, that hyper-Rayleigh fading is more common in metallic cavities than previously thought. Wireless sensor nodes operating in such an environment are likely to be static and unable to move out of severe fades. As such, static nodes may need to use other diversity strategies in order to cope with severe fading. There are several diversity techniques in common use that attempt to mitigate small-scale fading; however, most studies examining gain for diversity techniques do so with respect to a Rayleigh fading environment. Exploring the gain of typical diversity techniques in a hyper-Rayleigh environment is a natural extension of gain studies already conducted within Rayleigh environments and the work presented in Chapter 3. This chapter was presented at the 2006 IEEE Wireless and Microwave Technology Conference (WAMI '06).

4.2 Compact and Simple Diversity Methods for Mitigating Severe Fading

4.2.1 Abstract

Recently, measured channel responses for wireless links in airframes, buses, and rotary aircraft environments have demonstrated that frequency-selective fading can be more severe than predicted by the Rayleigh channel model. The work herein investigates simple diversity methods as a means to mitigate such fading which is referred to as exhibiting hyper-Rayleigh behavior. In particular, the work presents the gains achieved by utilizing selection diversity for two spatially separated antennas and by simple phasing

of a two-element array. The key results are that (1) severe fades are well-mitigated in selection diversity even if elements are spaced less than the $\lambda/2$ typically assumed for statistically independent paths, and (2) even coarse phasing (increments of 45°) of elements mitigates severe fades. The motivation for this work is to develop diversity strategies suitable for use by low-energy wireless sensor nodes deployed in such severe environments; that is, the methods should be computationally simple, physically compact, and require minimum DC power to implement.

4.2.2 Introduction

Wireless sensor networks (WSN) have recently garnered much attention due to their numerous potential applications. Generally speaking, WSN are seen as an enabling technology for distributed monitoring of industrial, military, and natural environments. Much of the progress associated with WSN has focused on hardware and algorithm efficiency as a means to reduce power consumption and increase battery life. While system longevity is a significant issue, another common problem afflicting WSN technology is communications connectivity. Many applications, especially those that involve an immobilized system, may experience severe frequency-selective fading as a consequence of location specific multipath interference. To mitigate such fades in mobile communication systems, diversity strategies utilizing multiple signal paths with independent fading phenomenon have been implemented [1]. One method employs algorithms and multiple receiver chains to combine signals that are diverse in time (i.e., RAKE receiver). Likewise, the M signals available from an M -element antenna array can be either selected amongst or combined to mitigate fades. For sensor nodes, however, the

complexity and energy needs of a RAKE receiver exceed their capabilities. Furthermore, the requisite spacing assumed for multi-element antennas (i.e., $\lambda/2$) results in a physical package too large to be appropriate for sensor nodes. Also, methods that required fine tuning of antenna element phases and amplitudes (i.e., maximum ratio combining – MRC) are inappropriate for these energy-constrained systems.

Another diversity technique utilizes M different frequencies either on a stand-by or in a coordinated fashion. This method is effective since frequencies separated by more than the coherence bandwidth of the channel will experience uncorrelated fading [1]. Frequency diversity does require that the bandwidth (i.e., extra channels) be available. Furthermore, frequency diversity would require coordination and synchronization amongst the many sensor nodes to choose an appropriate single frequency. An alternative is for individual sensors to be allocated a unique frequency, but this would be spectrally inefficient for the many applications in which the data rates are expected to be very low. However, for high rate applications (e.g., accelerometer data from multiple nodes), strategies have been proposed for such allocation of spectrum in both single and multiple frequency systems [2].

Most diversity studies have been conducted in the context of mobile wireless applications and thus have assumed the worst case fading environment to be Rayleigh. Conversely, many WSN application nodes will be statically deployed in enclosed environments (e.g., aircraft, shipping containers, buildings) that may exhibit frequency-selective fading that is more severe than predicted by the Rayleigh channel model (that is, hyper-Rayleigh fading [3]). Our interest is to illustrate the effectiveness of diversity

methods in mitigating such severe fading in these environments.

Herein, we are concerned with systems whose operational frequency have been pre-allocated but may result in deep fading for some of the nodes. In particular, we are motivated in this work to investigate methods that are (1) effective in mitigating such severe frequency-selective fades and (2) are suitable for use by wireless sensors. This work presents empirical results illustrating two different antenna diversity schemes that meet these objectives. Testing was conducted in the 2.4 GHz ISM band which is of interest to wireless sensors applications predominantly due to the IEEE 802.15.4/ZigBee standards and available radio chipsets.

4.3 Spatial/Polarization Diversity Gains

For multi-element antennas designed for the purpose of mitigating fades, the common convention is that elements should be spaced $\lambda/2$ or greater where λ is the carrier wavelength. This criterion assumes a Rayleigh fading channel for which the spatial correlation coefficient has been shown to be [4]

$$\rho = J_0(\beta d) \text{ where } \beta = \frac{2\pi}{\lambda} \quad (4.1)$$

From (4.1) the elements will receive statistically independent signals in terms of fading phenomenon, i.e., $\rho = 0$, when the element separation $d = \lambda/2$. However, for systems operating at 2.4 GHz, this distance corresponds to ~ 6 cm which is relatively large in comparison to the dimensions foreseen for a wireless sensor. For example, the Crossbow Mote currently used in many research programs has dimensions of 5 cm x 3 cm, and may present a challenge to antenna packaging.

To address issues related to packaging constraints, our objective was to ascertain whether antenna element spacing more compact than $\lambda/2$ would yield diversity benefits. For our tests, omni-directional antennas were placed inside a RF screen room located at the University of Vermont (UVM). Three locations within the cage which exhibited hyper-Rayleigh fading were chosen. A spectrum analyzer with tracking generator was connected to the two antennas to conduct the measurements. Data collected were frequency sweeps from 2.40-2.45 GHz. At each of the three locations, the receive antenna was placed in 16 positions spaced at 1cm increments, while leaving the transmit antenna fixed. This data thus consisted of 48 power versus frequency measurements examples of which can be seen in the left panels of Figure 4.1 and Figure 4.2.

This data can also be represented in terms of fading probability relative to the median signal strength as shown in the right panels of Figure 4.1 and Figure 4.2. These figures present the cumulative distribution function (CDF) for the measured data. In the example presented, the fading illustrated in Figure 4.1 is noted to be relatively benign with the exception of the 38 dB fade occurring at ~ 2.403 GHz. The CDF for this data illustrates that the probability of this fade exceeds that predicted by the Rayleigh fading model. As such, this would be an example of a hyper-Rayleigh fading channel. The measured data is also compared to the two-ray model which was proposed in [3] as an alternative worst-case scenario for severe fading environments but, as one can see, the measured case is not as severe as this. Moving the receive antenna 1 cm, however, is sufficient to mitigate this severe fade; the resulting measurement (Figure 4.2) exhibits Ricean statistics with no fade deeper than 6 dB relative to the median. Note that 1 cm is \sim

$\lambda/12$ significantly less than $\lambda/2$.

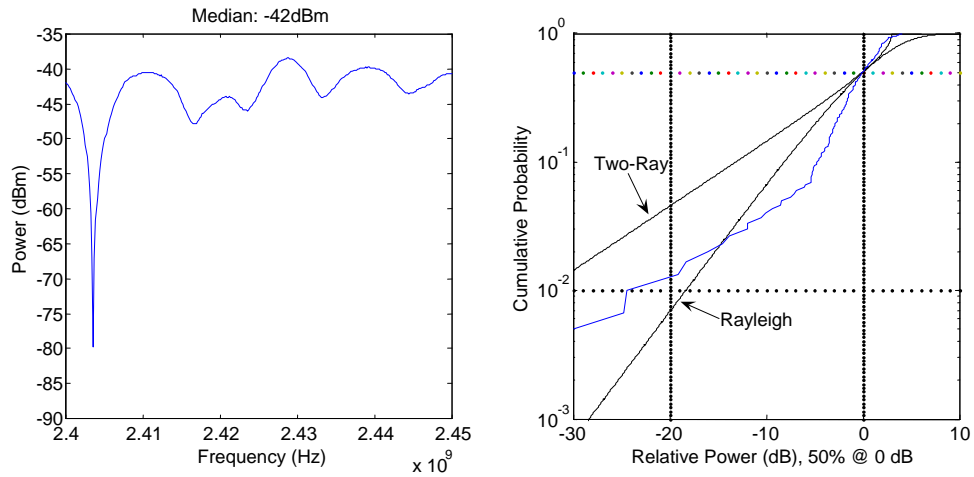


Figure 4.1. Spectrum and CDF depicting hyper-Rayleigh fading

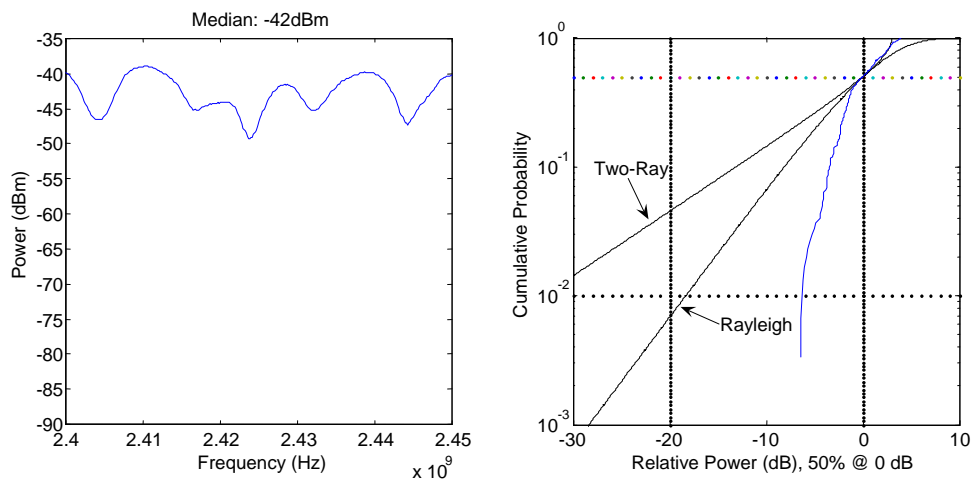


Figure 4.2. The deep (~38 dB) fade disappears when the received antenna is moved by 1 cm. At this location the fading now exhibits Ricean statistics.

Of the 48 locations measured, 19 exhibited deep fades. From the collected data, the spectrums that exhibited 20-30 dB and >30 dB fades from the median value were compared to the spatially adjacent spectrums (± 1 cm and ± 2 cm). The gain was determined by subtracting the power value at the point where the fade occurred from the

corresponding power value of the adjacent spectrum. In Table 4.1 a summary of the average gains (i.e., effectiveness of mitigation) is presented as a function of these separation distances.

Table 4.1. Spatial diversity gains for mitigating measured severe fades

Fade Depth	Number of Fades	Average Gain w/ 1 cm separation	Average Gain w/ 2 cm separation
20-30 dB	10	15.6 dB	20.6 dB
>30 dB	9	26.7 dB	32.8 dB

It can be ascertained from these results that, on average, the deep fades are effectively mitigated by spacing elements a distance of 2 cm ($\sim\lambda/6$). Our explanation for this great improvement over these short distances is that diversity paths need not be truly independent in severe environments. It has been shown that, for Rayleigh channels, antenna arrays utilizing selection diversity with correlations as high as 80% still have considerable gain over that of a single antenna [4]; this concept is illustrated in Table 4.2. While our results cannot be directly compared to Table 4.2 since we consider a range of fades, we do see that, overall, our measured gains in hyper-Rayleigh environments exceed those predicted for Rayleigh fading channels [4, 5]. This result was predicted through analysis in [4] but herein we provide empirical data to justify this point.

Table 4.2. Theoretical spatial diversity gains in Rayleigh environments

Fade Depth	Gain at 1 cm ($\rho=.9378$)	Gain at 2 cm ($\rho=.7629$)	Gain at $\lambda/2$ ($\rho=0$)
20 dB	6.0 dB	8.5 dB	11.0
30 dB	11.0 dB	13.0 dB	15.0

The effectiveness of mitigating fades given short separation distances motivated a study on simply utilizing collocated but orthogonally polarized antennas. In this study, fading data was collected at two polarizations for 36 different fading configurations. In this data set, over 50 fading events were noted. The majority of the deep fades were noted when the transmitter and receiver were co-polarized (V). As illustrated in Table 4.3, selecting between two orthogonal polarizations yielded significant diversity gains (again exceeding Rayleigh predicts, Table 4.2, $\rho=0$) in this highly multipath and highly depolarizing environment.

Table 4.3. Polarization selection diversity gains for mitigating measured severe fades

Fade Depth	Number of Fades	Average Gain
20-30 dB	42	18.1 dB
>30 dB	10	27.0 dB

4.4 Coarse Phase Combining Gains

Instead of selecting between signal paths as discussed in Section 4.2, the statistically independent paths can be combined in phase to maximize the resulting signal. This approach, maximum ratio combining (MRC), requires the wireless device to have the ability to continuously (in time and magnitude) adjust amplitudes and phases of the M paths. This approach is known to provide superior diversity gains as compared to selection diversity. However, the complexity and energy requirements of this approach are difficult to justify for nominally static environments. As such, this work considered a simpler design of an $M = 2$ element antenna where the phase in one path could be adjusted in coarse increments of 45° . The antenna, developed by the co-authors at the University of South Florida (USF), has three features to assist in fade mitigation: (1)

antenna elements that are spatially separated by $\lambda/2$, (2) elements that are spatially oriented orthogonal to each other and (3) a coarse phase shifter inline with one of the elements. The two paths are combined using a 3-dB hybrid. The antenna is depicted below in Figure 4.3.

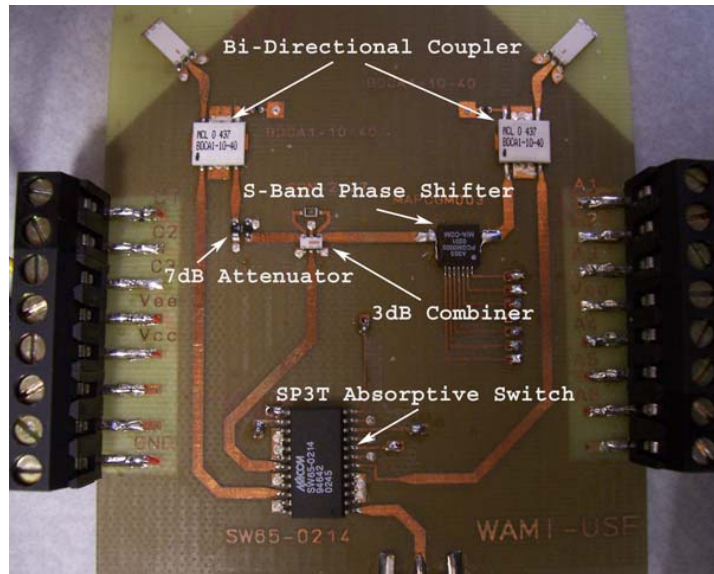


Figure 4.3. Simple two-element array utilized for coarse phase combining study

Similar to the earlier test, a location was chosen that exhibited hyper-Rayleigh fading. From this location, measurements from 16 positions - each 1 cm apart - were taken. At each position, measurements were collected while the USF antenna used phase shifts from 0° to 315° in 45° increments (i.e., 128 measurements in total).

Figure 4.4 depicts the spectrum received when the two elements were summed without introducing a phase into either. As can be seen, the figure is characterized by deep fades of 25 dB. In addition, the median received power is -58 dBm. Figure 4.4 depicts the spectrum received when the two signals were summed after introducing a

180° phase into one of the elements. The resulting change is significant. The spectrum is relatively flat with fades no larger than 6 dB relative to the median which has increased 9 dB to -49 dBm. From the CDF, the new spectrum follows Ricean fading.

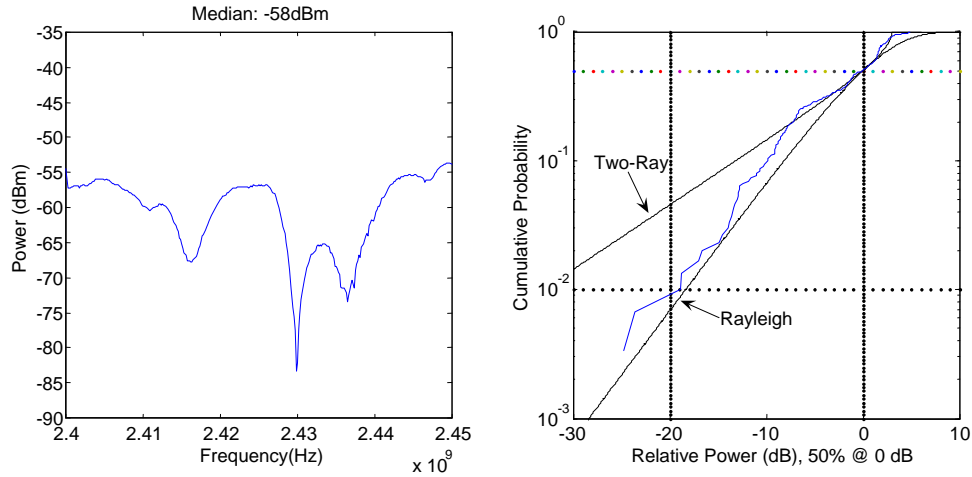


Figure 4.4. Two element antenna array with 0° phase shift

Obviously, the entire spectrum depicted in Figure 4.5 is much better to operate within than the one depicted in Figure 4.4. However, for single channel systems the objective would be to optimize only the allocated bandwidth, not the entire spectrum. In Table 4.4 we illustrate the phase shifts required to mitigate such band fades. Our criteria for a mitigated fade was that it be no more than 6 dB below the median received value. From our data, the vast majority of fades were mitigated by coarse shift up to $\pm 90^\circ$. Equipping a stationary wireless sensor node with this type of antenna would allow it to significantly mitigate the fading effects from multipath without large antennas or complex algorithms, thereby making this technique very effective.

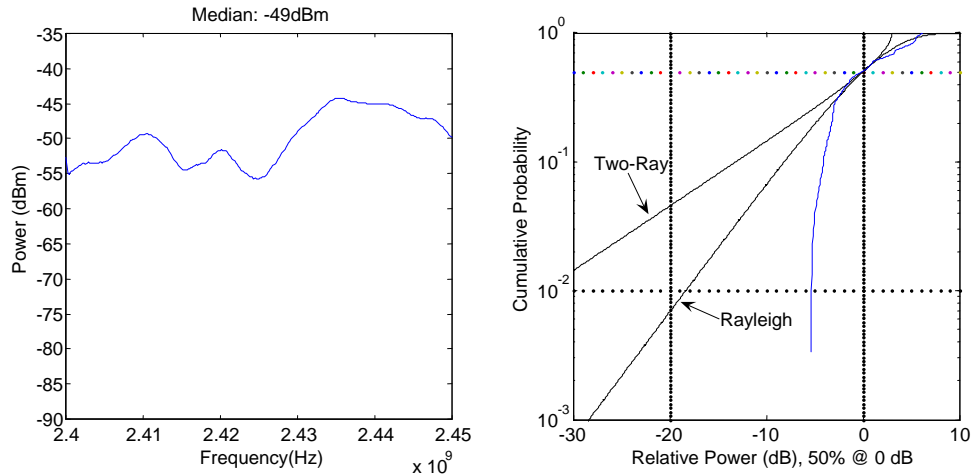


Figure 4.5. Two element antenna array with 180° phase shift on one element

Table 4.4. Phase shifts required to mitigate severe fades

Fade Depth	Number of Fades	±45°	±90°	±135°	±180°
20-30 dB	30	56.5%	26.5%	10.0%	7.0%
>30 dB	8	62.5%	12.5%	12.5%	12.5%

4.5 Conclusions

In this chapter, we have presented results of an initial investigation in which we measured the effectiveness of simple diversity methods in mitigating hyper-Rayleigh fading environments. The work considered only the 2.4 GHz ISM band which is of special interest to WSN that may employ the IEEE 802.15.4 standard or possibly the IEEE 802.11b/g standard. The results showed that severe fading could be mitigated using an element spacing significantly less than $\lambda/2$. This is important specifically with respect to the ever decreasing size of WSN nodes. The results have also illustrated that a simple diversity method such as a 2-element antenna array with a phase shifter can significantly mitigate severe fades. Based on these results, we have additionally

investigated the performance of extremely small form factor antennas (spacing $< \lambda/4$) in conjunction with coarse phase shifters.

The authors would like to acknowledge the Goodrich Corporation's Aerospace Lighting Systems Group of Oldsmar, FL and Fuel and Utility Systems Group of Vergennes, VT, for their support of this research.

4.6 References

- [1] Rappaport, T. *Wireless Communications, Principles and Practice*, 2 ed., Prentice Hall, 2002.
- [2] Galbreath, J. and J. Frolik, "Channel allocation strategies for wireless sensors statically deployed in multipath environments," Fifth International Conference on Information Processing in Sensor Networks (IPSN06), April 19-21, 2006, Nashville, TN.
- [3] Frolik, J. "A case for considering hyper-Rayleigh fading channels," IEEE Trans. Wireless Communications, Vol. No. 6, Issue 4, April 2007.
- [4] Jakes, W. *Microwave Mobile Communications*, John Wiley & Sons, Inc. 1974
- [5] Schwartz, M., B. Bennett, and S. Stein, *Communication Systems and Techniques*, McGraw-Hill Book Company 1966

CHAPTER 5: RESULTS FROM ADDITIONAL ANTENNAS

The results from Chapter 4 have shown that severe fading could be mitigated using an element spacing significantly less than $\lambda/2$. This is important specifically with respect to the ever decreasing size of WSN nodes. The results have also illustrated that a simple diversity method such as a two-element antenna array with a phase shifter can significantly mitigate severe fades.

In short, simple mitigation methods hold promise in severe fading environments. In this chapter we extend these results to investigate whether more compact or simpler designs will also be effective in mitigating these fades. In particular we present results from two additional antennas. The first equally combines the two diversity paths spaced $\lambda/2$ without any phase adjustments. The second has an element spacing of $\lambda/4$, smaller than the $\lambda/2$ typically employed for statistical independence.

5.1 Passive Combining with $\lambda/2$ Element Spacing

The antenna created by USF for this course of study utilizes passive combining of two paths and some degree of selection diversity. Figure 5.1 depicts the antenna and its simple design, which includes two chip antenna elements oriented orthogonally to each other and spaced $\lambda/2$ or approximately 6 cm apart. Both spacing and orientation are included in order to maximize element independence. Two 3dB splitters are inline with each element which are used to route half of the received power to the 3 dB combiner for the combined path and the other half to the element port. Three terminals are also provided which allow each chip antenna to be monitored independently along with the combined path.

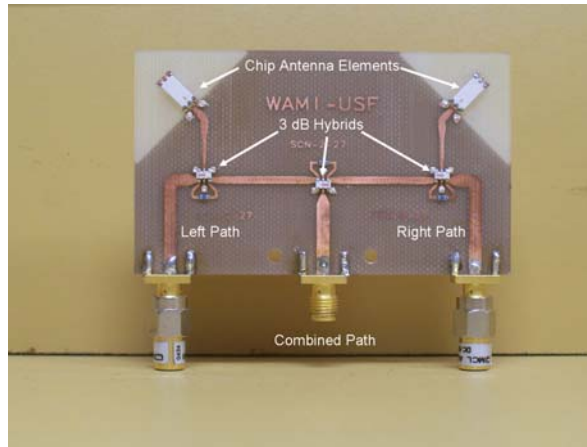


Figure 5.1. Passive combining with $\lambda/2$ element spacing

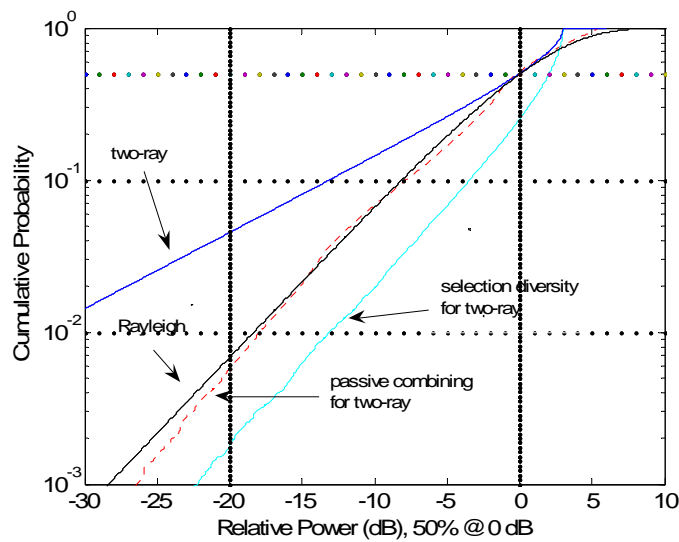


Figure 5.2. Simulated diversity gains

The antenna works by simply combining the two individual paths from each antenna element. In theory, by adding the two paths together, the stronger signal should make up for any fading experienced by the other as long as they experience uncorrelated fading. Figure 5.2 depicts the simulation results for the diversity gain provided through

passive combining and selection diversity. Originally, both elements experienced a two-ray fading environment which, as shown, was improved through utilizing either of the two diversity techniques.

Ostensibly, this antenna could be utilized by limiting access to only the combined path; however, this can worsen the fading, as will be shown. Another mode with which the antenna can be utilized is to electronically switch between the three ports, searching for the best signal strength at a given frequency. Allowing for selection diversity increases flexibility and the likelihood a severe fade can be mitigated. Table 5.1 summarizes the results of performance tests in which the antenna used selection diversity techniques. The table describes the average gain due to switching between different elements (between the right and left, combined path and left, and combined path and right). Table 5.1 illustrates that selection diversity in conjunction with simple passive combining may offer a significant diversity gain for wireless systems. For example, if a fade is experienced on the left element, the hardware can be expected to gain about 24.8 dB by switching to the combined path for fades in the 20 – 30 dB range and 39.1 dB for fades > 30 dB. Table 5.1 also shows that utilizing the combined path gave the greatest diversity gain for the deepest fades (39.1 dB for > 30 dB), and that utilizing both elements alone also provided significant gains. Using the left and right elements alone provided a superior gain of 27.4 dB for fades within the 20-30 dB range and a diversity gain of 37.5 dB for fades greater than 30 dB; this is better than the combined path to right element statistics.

Table 5.1. Selection diversity and passive combining

Fade Depth	Number of Fades	Right - Left Average Gain	Combined - Left Average Gain	Combined - Right Average Gain
20-30 dB	42	27.4 dB	24.8 dB	24.6 dB
> 30 dB	14	37.5 dB	39.1 dB	28.1 dB

Table 5.2. Channel characteristics for the right, left, and combined paths

Data Set	Antenna Port	Rician (%)	Rayleigh (%)	Hyper-Rayleigh (%)
DatasetOne	Combined	68.75	12.5	18.75
	Right	50	18.75	31.25
	Left	93.75	0	6.25
DatasetTwo	Combined	62.5	0	37.5
	Right	75	0	25
	Left	62.5	18.75	18.75
DatasetThree	Combined	75	6.25	18.75
	Right	62.5	6.25	31.25
	Left	75	6.25	18.75

Table 5.2 shows the environment characteristics experienced by the antenna through the right element, left element and the combined path. From the table, it can be seen that the combined path may experience a larger percentage of fading classified as hyper-Rayleigh than the other two paths. This occurred in the case of DatasetTwo, where the combined path experienced a channel characterized as hyper-Rayleigh 37.5% of the time, as compared to 25% for the right element and 18.75% for the left element. As such, it seems that solely relying on the combined path is not advisable.

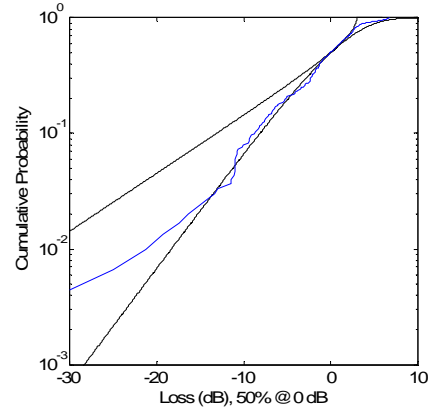
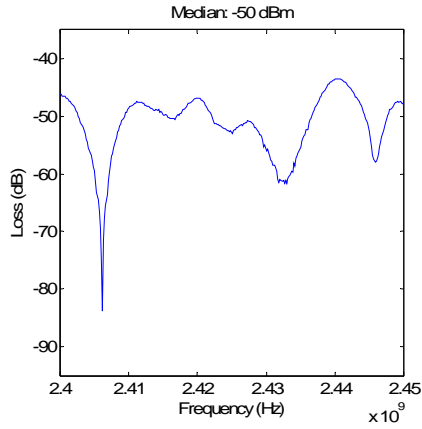


Figure 5.3. Two element passive antenna (right element)

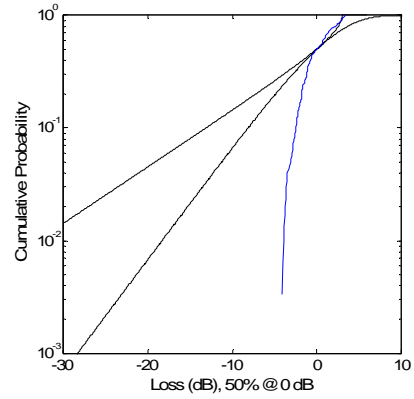
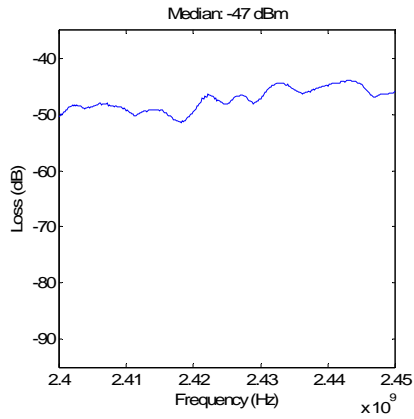


Figure 5.4. Two element passive antenna (left element)

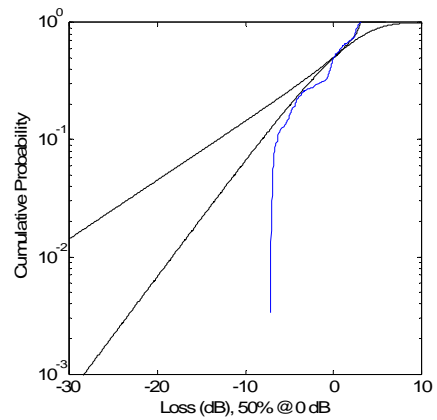
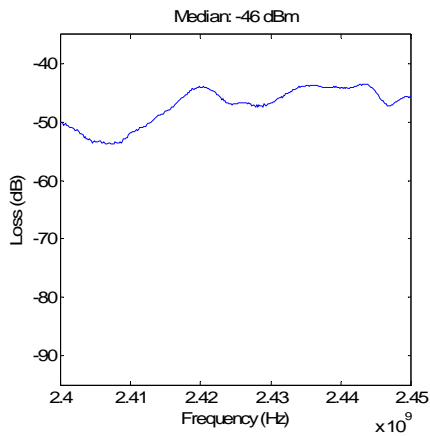


Figure 5.5. Two element passive antenna (combined path)

The diversity gains described in Table 5.1 are only associated with the fade ranges described (i.e., 20 – 30 dB and > 30 dB) and not the entire band as Table 5.2 describes. Although not occurring at the same frequency as the left and right path, the combined path exhibits significant fades despite the diversity gains. In essence, having the combined path as a selection option will be a benefit, but solely relying on the combined path to mitigate hyper-Rayleigh fading is not. As an example of the diversity gain benefit for the passive antenna, Figure 5.3 illustrates a severe fade of over 30 dB which is clearly hyper-Rayleigh. The in-band response becomes much more benign by simply switching from the right element to the left element, resulting in a Rician environment (depicted in Figure 5.4). In contrast, the combined path, shown in Figure 5.5, has a mild fade at the same frequencies as, and a better fading environment overall than, the right element. However, the fading environment for this path is worse than that of the left element.

5.2 Coarse Phase Combining with $\lambda/4$ Element Spacing

The empirical results from Chapter 4 showed that severe fading may be mitigated using an element spacing significantly less than $\lambda/2$. To this end, USF fabricated another antenna, altering the element spacing to $\lambda/4$. Figure 5.6 depicts the antenna with $\lambda/4$ element spacing. The antenna is similar to the $\lambda/2$ antenna depicted in Figure 4.3 in design, with the exception of the element spacing.

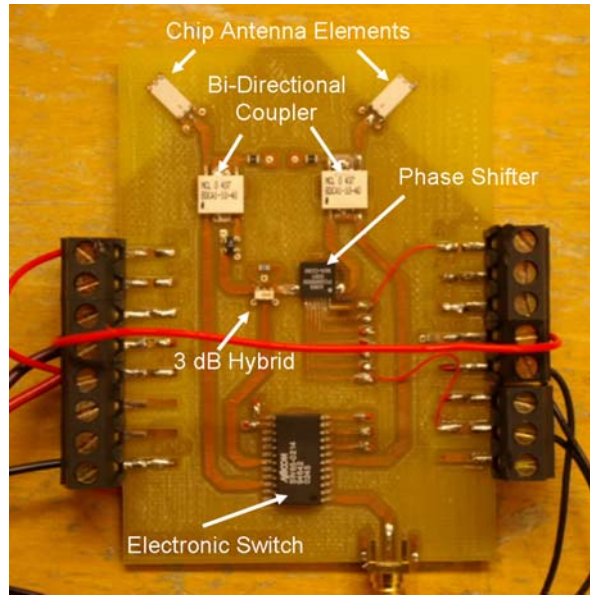


Figure 5.6. Prototype antenna with $\lambda/4$ separation

5.2.1 Test Setup

To conduct the tests, the antenna was positioned adjacent to a rotational-positioner which turned a broomstick with 1 square foot of sheet metal attached to it. The positioner was rotated 10° for each increment; this allowed for the creation of 36 ($360^\circ/10$) distinct fading environments within the same test setup, thereby eliminating the need for multiple testing locations. For each increment, a tracking generator in conjunction with a 2.4 GHz band omni directional antenna (TX) and the $\lambda/4$ USF antenna (RX) were used to sweep the channel. As depicted in Figure 5.7, a Freescale MC13192-EVB supplied power through a custom designed external power supply and controlled the phase shifter via the general purpose IO (GPIO). A 2.4 GHz omni directional antenna was attached to the Freescale board and positioned through a small opening in the screen room to facilitate wireless communication with the computer. Utilizing a graphical user

interface (Figure 6.4) to wirelessly increment the phase shifter (described later in Chapter 6), eight in-band sweeps were recorded - one for each phase, 0° through 315° , in 45° increments. In all, there were 288 in-band plots. Each plot had zero or more deep fades from which diversity gain information could be acquired.

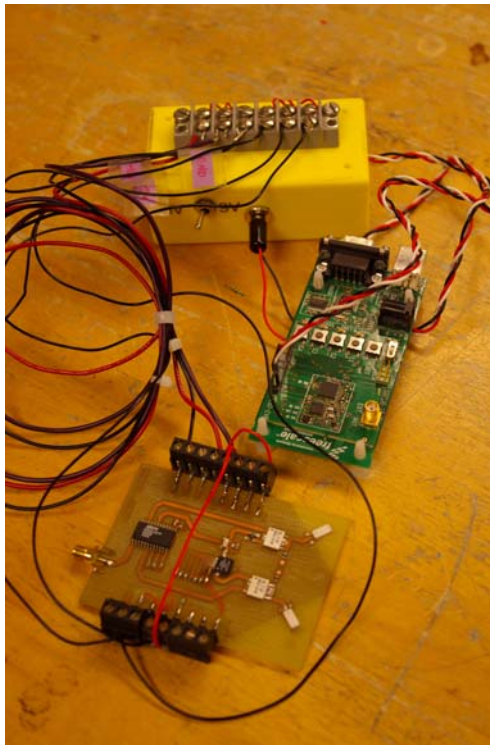


Figure 5.7. Quarter wavelength test components (power supply, controller, and antenna)

5.2.2 Analysis

Table 5.3 presents the average gain for each phase shift of the quarter wavelength antenna. If the diversity gains are evaluated by the criteria defined in Chapter 4, very few of the deep fades encountered can be considered mitigated. This is to say that the gain associated with using the phase shifter was not large enough to bring the fade to within 6 dB of the median received power. As such, the average (mean) gain of each phase shift

is given rather than the percentage of the fade that each phase shift was able to mitigate. As can be seen, all phase shifts contribute similarly toward the gain, varying by only about 2 dB or less.

Table 5.3. Average gain for the quarter wavelength antenna

Fade Depth	Number of Fades	+/- 45°	+/- 90°	+/- 135°	+/- 180°
20-30 dB	122	5.8 dB	6.4 dB	6.5 dB	4.5 dB
> 30 dB	19	15.8 dB	19.0 dB	18.1 dB	17.2 dB

Table 5.4. Average gain for the half wavelength antenna¹

Fade Depth	Number of Fades	+/- 45°	+/- 90°	+/- 135°	+/- 180°
20 - 30 dB	20	23.4 dB	27.2 dB	28.3 dB	28.7 dB
> 30 dB	5	41.7 dB	45.3 dB	46.6 dB	40.0 dB

As a point of comparison, the average gains for the $\lambda/2$ coarse phase shifting antenna are presented above in Table 5.4. For the 20 to 30 dB fade category, the $\lambda/4$ antenna provides a diversity gain between 4.5 and 6.5 dB, a gain of 16.9 to 24.2 dB less than that of the $\lambda/2$ antenna. Likewise, for the >30 dB fade category, the $\lambda/4$ antenna provides a diversity gain between 15.8 and 19.0 dB, less than the $\lambda/2$ antenna by between 21.0 and 30.8 dB. Whereas the $\lambda/2$ antenna is capable of fully mitigating severe fades, the $\lambda/4$ antenna cannot. That being said, our results for the $\lambda/4$ antenna still show potential benefit for severe fading environments.

It is possible that coupling within the antenna substrate causes the $\lambda/4$ elements

¹ Fades were counted twice for Table 4.4 to take into account that a fade could be mitigated using positive and negative phase shifts. For example, if a fade occurs with a phase shift of 135° and is mitigated by 180° and 90° (+45° and -45° referenced to 135°, respectively), the fade would be counted as two fades, one for each situation. Table 5.4, like Table 5.3, is only concerned with average gain per phase shift and not which phase or phases mitigate the fade of interest; thus, each phase is counted once.

to experience correlated fading behavior thereby reducing the diversity effects; this hypothesis, however, has not been fully investigated. In Chapter 4, the spatial diversity data was collected with a single antenna and thus no coupling between measurements was possible. More steps should be taken to make the elements in the antenna independent from one another.

5.2 Conclusion

Despite the empirical and theoretical evidence presented in Chapter 4, the experiments described in this chapter have shown that using only passive combining is ineffectual and sometimes worse than simply using an omni-directional antenna. These empirical results contradict simulation results; this discrepancy calls for further investigation. The $\lambda/4$ antenna was an improvement over the passive antenna but, as predicted based on an expectation of increased correlation between paths, it performed poorly compared to the $\lambda/2$ antenna. Nonetheless, the $\lambda/4$ antenna did have a significant diversity gain when experiencing severe fades and could still be used to reduce the severity of the fades with half of the footprint required by the $\lambda/2$ antenna. This antenna may be a necessity for static nodes with limited space and energy requirements deployed in metallic cavities.

CHAPTER 6: INTEGRATING A DIVERSITY ANTENNA WITH HARDWARE

6.1 Foreword

This chapter demonstrates the use of the half wavelength, two-element, phased combining antenna in conjunction with a wireless sensor. The diversity gain of the antenna within a hyper-Rayleigh environment was thoroughly examined in Chapter 4 and its derivatives in Chapter 5. Chapter 6 will show that a wireless sensor is indeed able to utilize a low complexity combining antenna and exhibit a significant increase in link-quality in severe environments. This demonstration was presented at the sixth international conference on Information Processing in Sensor Networks (IPSN '07). The work presented herein also appears in the IPSN '07 proceedings.

6.2 Integrating a Diversity Antenna with Hardware

6.2.1 Abstract

This demonstration presents the results of a study to address an issue which has constrained the effectiveness of wireless sensor network deployments to date: connectivity. A diversity antenna has been developed that is low in complexity and therefore suitably controlled using computationally-constrained wireless sensor hardware. This antenna demonstration utilizes an IEEE 802.15.4-compliant Freescale-based platform.

6.2.2 Introduction

For the progress made in wireless sensor networks during the past decade, demonstrations to date have yet to operate at levels requisite for the envisioned ubiquity. Shortcomings are especially noted in link range and quality. While time-selective

multipath fading is generally acknowledged for mobile wireless communication systems, little work has considered fading scenarios for wireless sensor networks. For static deployments, one may expect temporal changes to be minimal if the environment is relatively inactive. However, this does not preclude the existence of frequency-selective fading. For instance, fading inside cavity structures (e.g., airframes) has been demonstrated to be more severe than would be predicted using the Rayleigh fading model [1].

This demonstration presents the results of a study to address this issue. In particular, a computationally-light, compact diversity antenna has been developed to mitigate frequency-selective fading. While this design is sub-optimal in comparison to diversity schemes employed in resource-rich wireless systems, we find the approach significantly improves connectivity of nodes operating in severe multipath environments. Additionally, it is appropriate for resource-limited sensor nodes due to its easy implementation. As an example, our test results for the prototype illustrate that fades on the order of 20-30 dB are easily mitigated across the 2.4 GHz ISM band [2]. In the proposed demonstration, the control of this prototype is performed with a ZigBee compliant, Freescale development board (Figure 6.1).

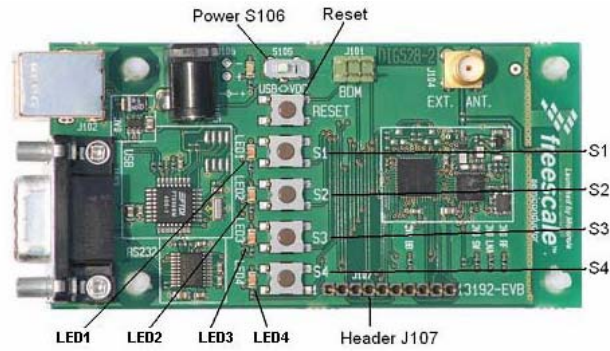


Figure 6.1. Freescale MC13192-EVB

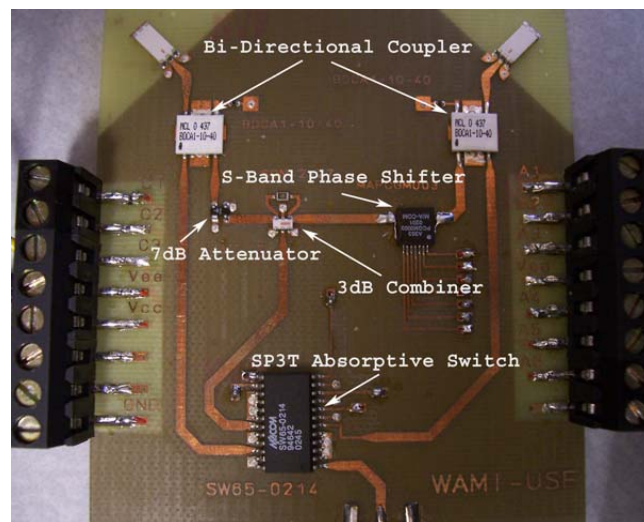


Figure 6.2. Low-complexity diversity antenna

6.3 Diversity Antenna Design

The antenna, developed in collaboration with the University of South Florida (USF) [2], has three features to assist in fade mitigation: (1) two antenna elements are spatially separated by $\lambda/2$, (2) these elements are spatially oriented orthogonal to each other, and (3) a coarse phase shifter is placed inline with one of the elements. The signals received from the two elements are combined using a 3-dB hybrid. To limit the I/O

requirements to three pins, the phase shifter is controlled in eight coarse increments of 45° (although the prototype’s phase shifter does enable finer granularity). Each chip antenna element has a peak gain of 3dBi. The antenna is depicted in Figure 6.2.

6.4 Demonstration Overview

Our demonstration of this diversity antenna utilizes three wireless sensor nodes. Two of the nodes have 5dBi omni-directional antennas. One node acts as coordinating node and the other as point of comparison (Omni-node). The third node is equipped with the adaptive antenna (USF-node). The coordinating node is controlled via a MATLAB script illustrated in Figure 6.3 and Figure 6.4.

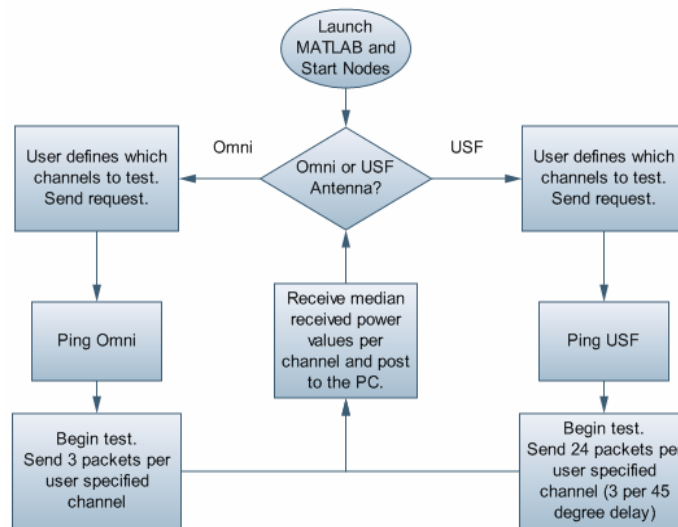


Figure 6.3. SPOTS demonstration routine

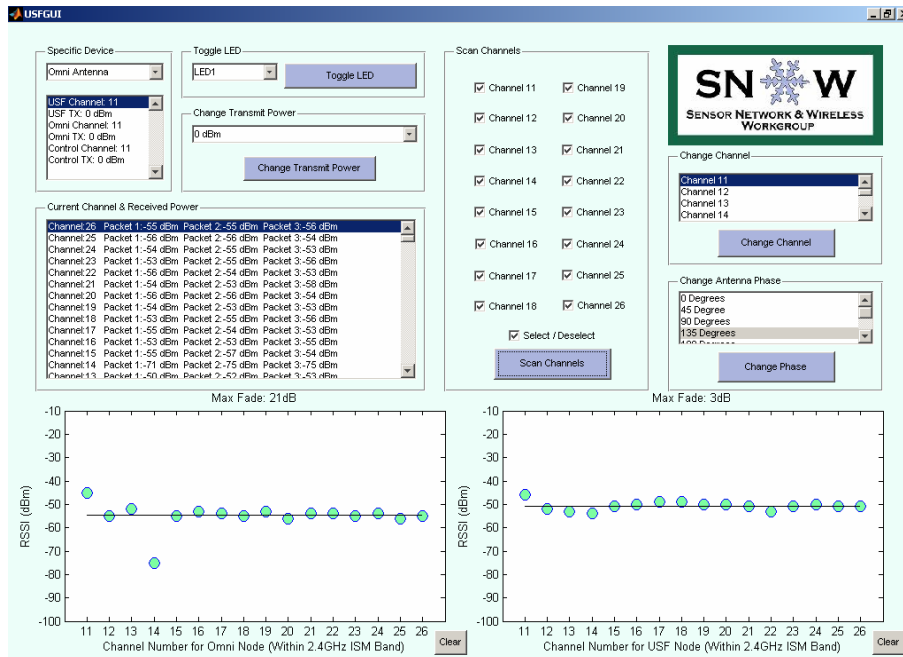


Figure 6.4. IPSN graphic user interface

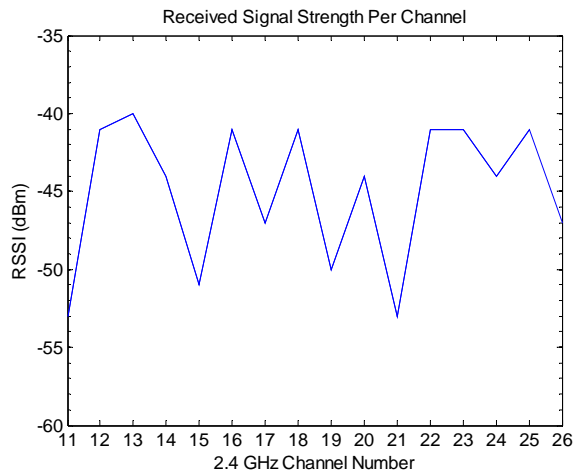


Figure 6.5. Example frequency selective fading

To characterize the Omni-node, the RSSI (received signal strength indicator value) is collected for three packets from each of the sixteen 802.15.4 channels. The Omni-node responds back to the coordinator with the median received power for each

channel tested and these values are presented through the MATLAB script (an example being illustrated in Figure 6.5).

A similar approach is taken to characterize the response of the diversity antenna enhanced node (USF-node). The Omni-node is physically replaced with the USF-node. For a given channel, the coordinator node sends 24 packets with the USF-node reconfiguring the antenna phase every three packets. Once all 24 packets are sent, the USF-node chooses the phase configuration that yields the best median received power for that channel. The test then moves on to the next channel and repeats until all desired channels have been tested.

6.5 Demonstration Details

A more detailed description of the test routine follows. Once the USF-node is powered on, it waits for a ping from the coordinating node to indicate that a test is being conducted. The ping will contain the channel numbers over which the test will be conducted and, once it is received, the USF-node will respond with an acknowledgment and begin waiting to receive the test packets. The node will wait until it receives three packets or times out, at which point it will find the median RSSI value, increment the phase delay by 45 degrees, and return to waiting for the next three packets. If the USF-node does not receive the test packets before it times out, the RSSI value will be stored as the MATLAB NaN (not a number) thereby indicating a dropped link. The phase will then be incremented and the process repeated. Once all eight phases have been cycled through, the USF-node will switch to the next channel, reset the phase delay to 0 degrees, and wait for the next three packets. This will repeat until all requested channels have

been tested. The USF-node will then respond to the coordinating node with the best RSSI value for each channel tested and the requisite phase delay. The coordinating node then outputs the data to the PC where it is plotted using MATLAB. At this point, the USF-node will return to waiting for the next ping from the coordinating node.

To fully illustrate the benefits of the antenna, the sensor nodes were placed in an open-ended copper mesh enclosure. This enhanced multipath reflections and, in doing so, created a frequency-selective fading environment. Under these conditions we have demonstrated that the antenna phase configuration changes in accordance with channel of operation. Furthermore, we have illustrated the antenna's ability to mitigate severe fades and to provide consistently flatter channel responses than an omni-directional antenna.

6.7 Demonstration of Graphic User Interface

The demonstration was controlled through a GUI developed in MATLAB. The GUI has the ability to conduct small tasks such as toggling LEDs, changing power, changing frequency, and adjusting the phase of the diversity antenna. The purpose of the demonstration was to run tests with the USF-node with the baseline Omni-node in order to compare their performances by conducting link quality tests. Both nodes were tested in the same location. Upon completion of the link quality test, the wireless node replied back with the results (e.g., the best median RSSI value and the associated phase configuration for each channel). The GUI then listed the RSSI value for each scenario (phase and channel) of the antenna over which the test was conducted, and plotted the best RSSI value for each channel.

6.8 References

- [1] Frolik, J. "A case for considering hyper-Rayleigh fading channels," IEEE Trans. Wireless Communications, Vol. No. 6, Issue 4, April 2007.
- [2] Ketcham, R., J. Frolik, B. Zivanovic, S. Melias, and T. Weller, "Effectiveness of simple diversity methods in mitigating hyper-Rayleigh fading environments," 2006 IEEE Wireless and Microwave Conference, Clearwater FL, December 4-5.

CHAPTER 7: CONCLUSION AND EXTENSIONS TO WORK

7.1 Significant Contributions of Work

The major contributions of the work presented herein are as follows.

- *Small-scale frequency-selective fading often exceeds the severity predicted by the Rayleigh fading model in metallic cavities.*

In Chapter 3, it has been shown that reliable communication is readily achievable with the median signal strength present in a cavity environment. Multipath is all but guaranteed, however, due to the cavity structure. The key conclusion of the investigation is that small-scale frequency-selective fading often exceeds the severity predicted by the Rayleigh fading model.

- *Simple diversity methods such as a 2-element antenna array with a phase shifter can significantly mitigate severe fades.*

The results in Chapter 4 showed that severe fading could be mitigated using an element spacing significantly less than $\lambda/2$. This is important specifically with respect to the ever decreasing size of wireless sensor nodes. The results have also illustrated that a simple diversity method such as a 2-element antenna array with a phase shifter can significantly mitigate severe fades. Based on these results, our current work is investigating the performance of extremely small form factor antennas (spacing $< \lambda/4$) in conjunction with coarse phase shifters. This future work is described further in Section 7.3.

- *Passive combining alone is not sufficient to protect against hyper-Rayleigh fading. An array antenna with a form factor of $\lambda/4$ contributes toward such protection by*

providing a significant diversity gain, though it is not as effective as the $\lambda/2$ antenna array.

The experiments described in Chapter 5 have shown that using only passive combining is ineffectual and sometimes worse than simply using an omni-directional antenna. This is partially due to the increased likelihood that the passive antenna will experience a severe environment (two elements vs. one element), but also due to the elements having a fading correlation greater than zero. Despite having less of a gain than $\lambda/2$ phased combining antenna, the $\lambda/4$ phased combining antenna array still had a significant diversity gain when experiencing severe fades and, as such, could be used to help mitigate the severity of the fades while reducing the footprint to half of what the $\lambda/2$ antenna would require.

- *Simple antenna arrays can be easily integrated with the wireless sensor node hardware.*

Although not an exhaustive example, Chapter 6 illustrated a proof of concept that the wireless sensor node could indeed utilize the antenna array. For a real-world deployment, the power supply would have to be integrated with that of the wireless nodes and the antenna would need to be on-board.

7.2 Current Work: CRCE Chamber

As presented earlier, recent empirical data collected in metallic cavities has indicated that it is not uncommon for the multipath fading within to be severe. While a means of categorizing and modeling hyper-Rayleigh fading has been developed, there are

no means to date which enable systems to be tested under reliable and repeatable scenarios [1]. In building test environments for wireless systems, two types of chambers, anechoic and reverberation, have traditionally been used. Current work presented herein describes the development of an alternative to anechoic and reverberation chambers: a compact, reconfigurable channel emulator (CRCE) chamber. The following sections introduce CRCE details which can be found in [1].

7.2.1 Chamber Test Environments for Wireless Systems

The anechoic chamber (Figure 7.1) is specifically designed such that RF energy incident on the walls is absorbed and not reflected. These chambers are normally used in EMC/EMI testing and for antenna measurements [1]. As a result of the absorptive wall material, multipath between a transmitting and receiving source is non-existent. For antenna testing, the chambers are often large enough to measure the far field antenna performance.

The reverberation or mode-stirred chamber (Figure 7.2) is also used for EMC/EMI testing but operates using different principles than the anechoic chamber. Instead of using absorptive material, the mode stirred chamber (MSC) utilizes highly reflective walls to form a resonant cavity in which the electric field is inhomogeneous. As the name implies, the MSC utilizes a metallic stirrer to disrupt the modes created by the resonant cavity, effectively averaging the field amplitude over time making the chamber nominally homogenous with field strength largely independent of location. The number of modes is determined by the size of the chamber and, since the chamber walls are conductors, must satisfy the zero electric field strength boundary condition. The number

of modes is the number of amplitude variations of the field at the cutoff frequency within the resonant cavity. MSC have been shown to be effective in creating time-varying environments with characteristics ranging from Rician to Rayleigh [1, 2].



Figure 7.1. Anechoic chamber testing a horn antenna²

Unlike the anechoic and mode stirred chambers, the CRCE chamber is used to create many different and repeatable fading scenarios (i.e., Rician, Rayleigh, or hyper-Rayleigh, to name a few) within its metallic cavity [1]. Since the motivation for the CRCE chamber is to emulate a given fading environment, the resonant cavity does not have to be large. For instance, a rule of thumb says that for effective mode stirring the MSC must have at least 60 modes (also known as an overmode environment) which is a length of about 30λ [3]. However, since the CRCE chamber is not concerned with field homogeneity, an overmode environment is rendered unnecessary.

² Courtesy of CSIRO located at: http://www.csiro.au/csiro/channel/_ca_dch2t.html

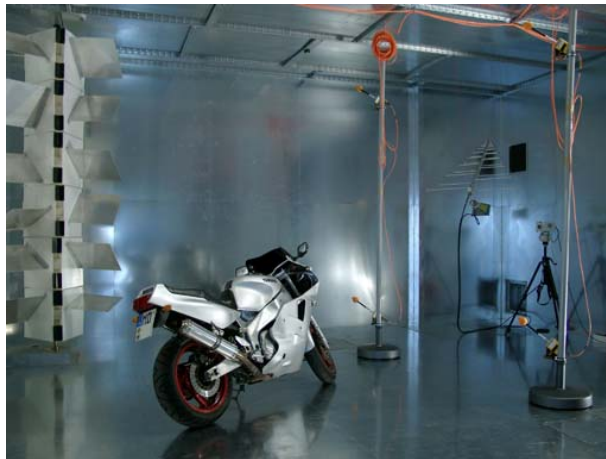


Figure 7.2. Reverberation chamber Otto-von-Guericke University, Germany

7.2.2 CRCE Chamber Design

The CRCE design is a box of dimensions 3' x 2' x 3' (height x width x length) currently used in conjunction with a two-port vector network analyzer (VNA) which sweeps and provides S-parameters for the frequency band of interest (in our case the band of interest is 2.4 GHz – 2.8 GHz) [1]. To mimic a larger fading environment, fixed coaxial delay lines can be added to the chamber to emulate strong reflections off of a distant object. Additional ports can inject an interference source for the purpose of conducting susceptibility tests. Finally, a reflecting blade attached to a stepper motor provides discrete control to a fixed number of fading scenarios.



Figure 7.3. Fabricated CRCE with oscillating fan

7.2.3 Example CRCE Fading Data

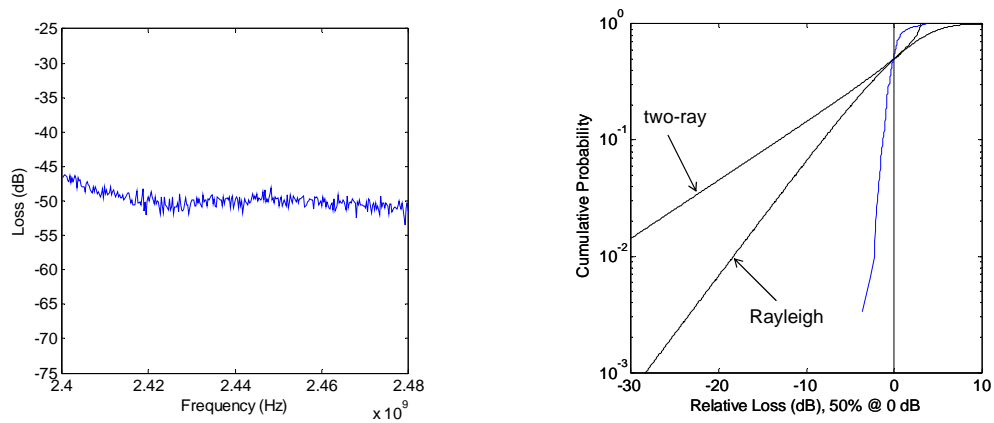


Figure 7.4. Frequency-selective fading response exhibiting Rician characteristics. In-band plot (left) and CDF plot (right).

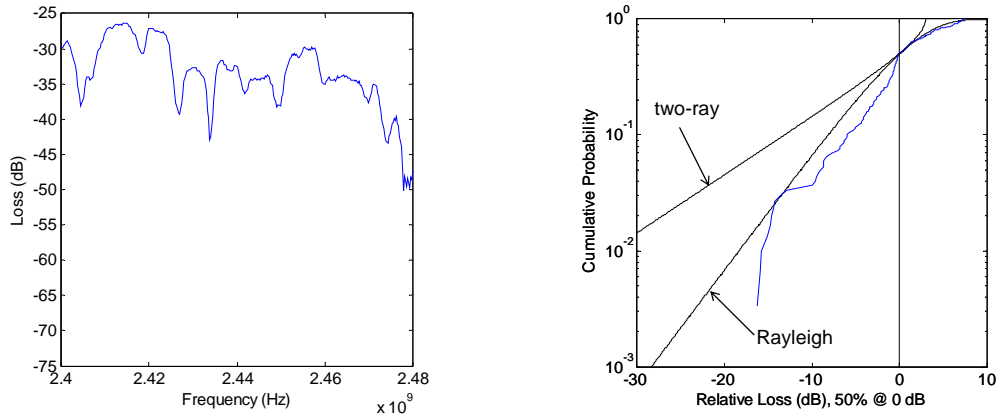


Figure 7.5. Frequency-selective fading response exhibiting Rayleigh-like characteristics. In-band plot (left) and CDF plot (right).

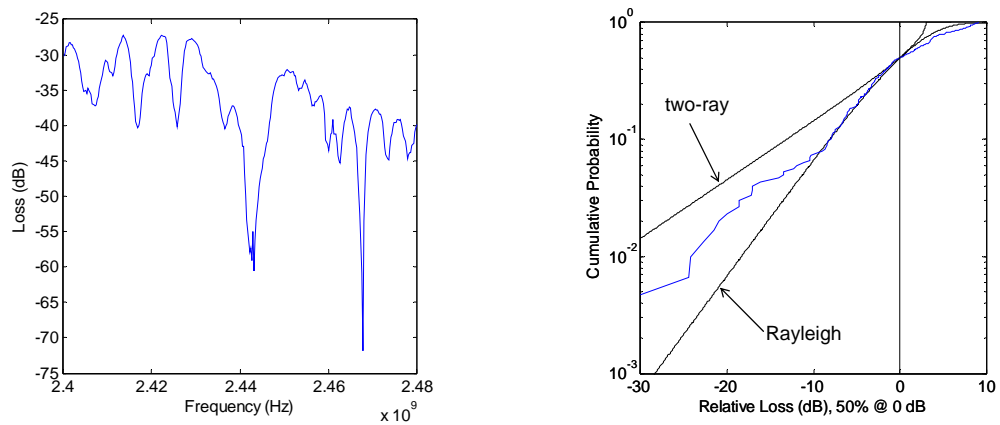


Figure 7.6. Frequency-selective fading response exhibiting hyper-Rayleigh characteristics. In-band plot (left) and CDF plot (right).

Our data consists of S_{21} (forward voltage gain) responses captured off of the VNA (Agilent MS2036A) and analyses of fading using CDF statistics. To illustrate the range of environments the CRCE chamber can provide, three channel scenarios are presented, each with their respective in-band and CDF plots. Figure 7.4 illustrates the ability of the CRCE chamber to emulate a relatively benign, Rician fading environment with an in-band variation of approximately 5 dB. Likewise, Figure 7.5 and Figure 7.6 illustrate a

progressively worsening environment exhibiting fading characteristics from Raleigh to hyper-Rayleigh, respectively. The CRCE chamber is able to provide an environment with severe fades like the approximate 40 dB fade in Figure 7.6. Each fading scenario is repeatable, enabling the CRCE chamber to test communication strategies under the same harsh conditions.

7.2.4 CRCE Conclusion

We have demonstrated that the CRCE chamber can fully emulate propagation characteristics from benign to severe in both frequency-selective and time selective fading scenarios. The utility of the CRCE chamber is rooted in its ability to emulate the most severe environments, supplying the wireless systems designer with an inexpensive tool for testing prototypes.

7.3 Future Work with Coarse Phase Combining

Chapter 4 has shown that coarse phase combining utilizing an antenna array with $\lambda/2$ spacing can be very effective in mitigating severe fading. In Chapter 5, data was presented showing that coarse phase combining coupled with an antenna array with $\lambda/4$ element spacing was less effective than the $\lambda/2$ spacing. Nevertheless, the quarter wavelength antenna still had significant diversity gain over no diversity technique when operating within a severe environment and would likely prove useful for static nodes operating in metallic cavities.

The last iteration of testing yet to be conducted involves an even smaller form factor: a zero spacing antenna array. The substrate for the new antenna is pictured in

Figure 7.7 without any attached components. Like the previous two coarse phasing antennas, this zero spacing antenna has a phase shifter, electronic switch, two bi-directional couplers, and two chip antennas. Unlike the other two antennas, in this iteration the elements are collocated, utilizing only their orthogonal orientation to create fading independence. It is probable that the antenna will follow the trend set by the other two antennas by providing less of a diversity gain overall. However, our main research interest is to determine whether this very compact antenna is effective against severe fades (>30 dB).

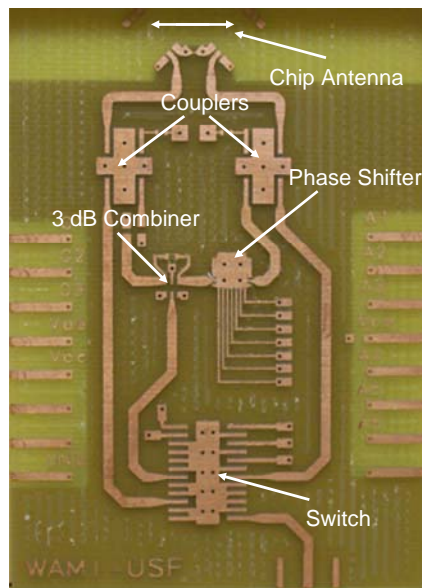


Figure 7.7. Prototype antenna with zero separation

7.4 Final Comments

Propagation characterization allows for the development of accurate models, such as the hyper-Rayleigh model, which offer key insight on the behavior of WSN within given environment. It is thus crucial to the development of wireless sensor systems with

high system reliability that propagation environments be fully characterized. Chapter 3 of this thesis has shown that the wireless propagation environment within a helicopter exhibits severe frequency-selective fading, illustrating that hyper-Rayleigh fading is more than a simple mathematical curiosity. Systems that are anticipated to operate within such an environment should adjust for this type of fading, beginning with modifications of the link budget.

While using the appropriate propagation model is necessary for a reliable system, diversity methods should also be considered. The performance of several simple diversity methods within such a severe environment has been studied and the methods have been shown to be effective in mitigating fades. For wireless sensor nodes operating in severe fading environments, the diversity gain may be considered worth the additional hardware and computation required to implement the technique. Such techniques could be used to strengthen link quality, increase the range of coverage, or even act as an “insurance policy” for closing the link.

The work presented in this thesis should provide a better understanding of the environment experienced by wireless sensors within a metallic cavity and establish a foundation upon which knowledge of the gains provided by simple diversity methods operating in such an environment can be built.

7.5 References

- [1] Distasi, S., S. Melais, R. Ketcham, et al. “A Compact, Reconfigurable Channel Emulator for the Study of Severe Multipath Fading,” Submitted to RWS 2008.
- [2] Holloway, C. et al, “On the use of reverberation chambers to simulate a Rician radio environment for testing wireless devices,” IEEE Trans. Antennas and Propagation, Vol. 54, No. 11, November 2006.

[3] Miner, G. *Lines and Electromagnetic Fields for Engineers*, Oxford University Press. 1996.

COMPREHENSIVE BIBLIOGRAPHY

- Akyildiz, I., W. Su, Y. Sankarasubramaniam and E. Cayirci, "Wireless sensor networks: a survey, *Computer Networks*," Volume 38, Issue 4, 15 March 2002, Pages 393-422.
- Chong, C-C. and S. Yong, "A generic statistical-based UWB channel model for high-rise apartments," *IEEE Trans. Ant. and Prop.*, Vol. 53, No. 8, August 2005, pp. 2389-99.
- Coleri, S., S. Y. Cheung, and P. Varaiya, "Sensor Networks for Monitoring Traffic," In *Forty-Second Annual Allerton Conference on Communication, Control, and Computing*, Univ. of Illinois, Sept. 2004.
- Distasi, S., S. Melais, R. Ketcham, et al. "A Compact, Reconfigurable Channel Emulator for the Study of Severe Multipath Fading," Submitted to RWS 2008.
- Durgin, G., T. Rappaport and D. de Wolf, "New analytical models and probability density functions for fading in wireless communications," *IEEE Trans. Communications*, Vol. 50, No. 6, June 2002.
- Estrin, D., L. Girod, G. Pottie and M. Srivastava, "Instrumenting the world with wireless sensor networks," In *Proc. Int'l Conf. Acoustics, Speech and Signal Processing (ICASSP 2001)*.
- Fitzhugh, C., J. Frolik, J. Covell, R. Ketcham, and T. Meyer, "2.4 GHz multipath environments in airframes," 2005 *Wireless and Microwave Technology Conference (WAMICON 2005)*, Clearwater, FL, April 7-8, 2005.
- Frolik, J. "A case for considering hyper-Rayleigh fading channels," *IEEE Trans. Wireless Communications*, Vol. No. 6, Issue 4, April 2007.
- Fubler, H. and S. Schnaufer, "Vehicular Ad-Hoc Networks: From Vision to Reality and Back," 4th *Annual IEEE/IFIP Conference on Wireless on Demand Network Systems and Services (WONS)*, Obergurgl, Austria, January 2007.
- Galbreath, J. and J. Frolik, "Channel allocation strategies for wireless sensors statically deployed in multipath environments," *Fifth International Conference on Information Processing in Sensor Networks (IPSN06)*, April 19-21, 2006, Nashville, TN.
- Haykin, S. and M. Moher, *Modern Wireless Communications*, Pearson Education, Inc. 2005.
- Holloway, C. et al, "On the use of reverberation chambers to simulate a Rician radio environment for testing wireless devices," *IEEE Trans. Antennas and Propagation*, Vol. 54, No. 11, November 2006.
- Jakes, W. *Microwave Mobile Communications*, John Wiley & Sons, Inc. 1974
- Joint Council on Aging Aircraft (JCAA), "A national strategy for aging aircraft," July 2004.

Ketcham, R., J. Frolik, B. Zivanovic, S. Melias, and T. Weller, "Effectiveness of simple diversity methods in mitigating hyper-Rayleigh fading environments," 2006 IEEE Wireless and Microwave Conference, Clearwater FL, December 4-5.

Ketcham, R., J. Frolik, and J. Covell, "Propagation characterization for in-aircraft wireless sensor systems," Transactions on Aerospace and Electronic Systems.

Lathi, B.P. Modern Digital and Analog Communication Systems, 3 ed., Oxford University Press, 1998.

Mainwaring, A., J. Polastre, R. Szewczyk, and D. Culler, "Wireless Sensor Networks for Habitat Monitoring," Proceedings of the 1st ACM International Workshop on Wireless Sensor Networks and Applications, September 28, 2002, Atlanta, Georgia, USA.

Miner, G. Lines and Electromagnetic Fields for Engineers, Oxford University Press. 1996.

MIT Technology Review, "10 emerging technologies that will change the world," MIT Technology Review, February 2003.

Petriu, E. "Sensor-Based Information Appliances," IEEE Instrumentation & Measurement Magazine. December 2000.

Poor, R. "Wireless Mesh Networks," Sensors Magazine, <http://www.sensormag.com>, February 1, 2003.

Pottie, G. and W. Kaiser, "Wireless integrated network sensors," Comm. ACM, 43(5):51-58, May 2000.

Rappaport, T. Wireless Communications, Principles and Practice, 2 ed., Prentice Hall, 2002.

Schwartz, M., B. Bennett, and S. Stein, Communication Systems and Techniques, McGraw-Hill Book Company 1966

Securaplane Technologies, Inc., Press Release, "Securaplane Technologies Awarded Boeing 787 Contract for Wireless emergency lighting, December 21, 2004, online: <http://www.securaplane.com/releases/pr0095.html> (21Nov06)

Securaplane Technologies, Inc., "Wireless Smoke Detection," online: <http://www.securaplane.com/smoke2.html>, Securaplane Technologies Inc. November 12, 2006.

Sensors Magazine, "UCSB Nanofabrication Facility Installs Wireless Monitoring System," Sensors Magazine, <http://www.sensormag.com>, May 9, 2006.

Sensors Magazine, "Web-Enabled Mesh Sensor Network Offers Remote PLC and Process Monitoring," Sensors Magazine, <http://www.sensormag.com>, April 26, 2006.

St. John, E. "Operational Issues Wireless Overview," presented at the World Airline Entertainment Association Single Focus Workshop (WAEA SFW), November 19-20, 2002, Washington DC.

Stankovic, J. and Q. Cao, "Wireless Sensor Networks for In-Home Healthcare: Potential and Challenges," in High Confidence Medical Device Software and Systems (HCMDSS) Workshop, Philadelphia, PA, June 2-3, 2005.

Tolle, G., J. Polastre, R. Szewczyk, and D. Culler, "A Macroscopic in the Redwoods," In Proceedings of the Third ACM Conference on Embedded Networked Sensor Systems (SenSys), 2005.

Waddoups, B., C. Furse and M. Schmidt, "Analysis of reflectometry for detection of chafed aircraft wiring insulation," Fifth Joint NASA/FAA/DoD Conference on Aging Aircraft, Orlando, FL 2001.

APPENDICES

APPENDIX A: ANTENNA CONFIGURATION FOR CHAPTER 3 TESTS

As noted in Chapter 3, for each of the six test locations in the helicopter, ~40 measurements were taken for different spatial and polarization configurations. Table A.1 details these configurations. *Total displacement* is in reference to the starting position along the equipment bay wall. Displacements were made normal to the link direction so as to minimally impact the transmitter-receiver distance (i.e., large-scale effects).

Table A.1. Small- and medium-scale test hub positions

Data set	Polarization	Total displacement (cm) from start
1/2	Vertical/Horizontal	0.0
3/4	Vertical/Horizontal	1.7
5/6	Vertical/Horizontal	2.5
7/8	Vertical/Horizontal	3.8
9/10	Vertical/Horizontal	5.0
11/12	Vertical/Horizontal	10.1
13/14	Vertical/Horizontal	15.2
15/16	Vertical/Horizontal	20.3
17/18	Vertical/Horizontal	25.4
21/22	Vertical/Horizontal	20.5
23/24	Vertical/Horizontal	50.8
25/26	Vertical/Horizontal	91.4
27/28	Vertical/Horizontal	111.7
29/30	Vertical/Horizontal	132.1
31/32	Vertical/Horizontal	172.7
33/34	Vertical/Horizontal	213.4
35/36	Vertical/Horizontal	254.0
37/38	Vertical/Horizontal	294.6
39/40	Vertical/Horizontal	335.8

APPENDIX B: THEORETICAL GAIN EQUATIONS FOR CHAPTER 4

Equation (B.1) provides the theoretical gains for two element selection diversity, as a function of fade depth and element correlation, in a Rayleigh fading environment [Jakes]. This result was utilized in Chapter 4 to offer a point of comparison; specifically, Table 4.2 and Table 4.3 presented the theoretical diversity gains within a Rayleigh environment. The theoretical gains were compared to the empirical gains of diversity techniques operating within a hyper-Rayleigh environment.

The probability that the resulting signal of a system using selection diversity will experience a SNR of less than or equal to γ_s is:

$$P_2(\gamma_s) = 1 - e^{-\frac{\gamma_s}{\Gamma}} [1 - Q(a, b) + Q(b, a)] \quad (\text{B.1})$$

Where Q is the Marcum Q Function, given by:

$$Q(a, b) = \int_b^{\infty} e^{-\frac{1}{2}(a^2+x^2)} I_0(ax) dx \quad (\text{B.2})$$

The Q function gives the probability that an observed value of random variable x will be greater than b , given the value of a . The variable x is a standardized Gaussian of zero mean and unit variance.

$$b = \sqrt{\frac{2\gamma_s}{\Gamma(1-p^2)}}, \quad a = bp \quad (\text{B.3})$$

p stands for the magnitude of the complex cross-covariance of the two fading Gaussian

signals; p^2 is very nearly equal to the normalized envelope covariance of the two signals.

$$\Gamma = \text{Average SNR} = \frac{E[\text{Signal Power Per Branch}]}{E[\text{Noise Power Per Branch}]} \quad (\text{B.4})$$

$$\gamma_s = \text{Individual Branch SNR} \quad (\text{B.5})$$

$$\frac{\gamma_s}{\Gamma} = \text{Fade Depth (Watts)} \quad (\text{B.6})$$

Figure B.1 resulted by plotting the cumulative probability in equation (B.1) with respect to the fade depth (equation (B.6)). This graph was utilized to find the diversity gain for a two-element selection diversity antenna with various element covariance coefficients.

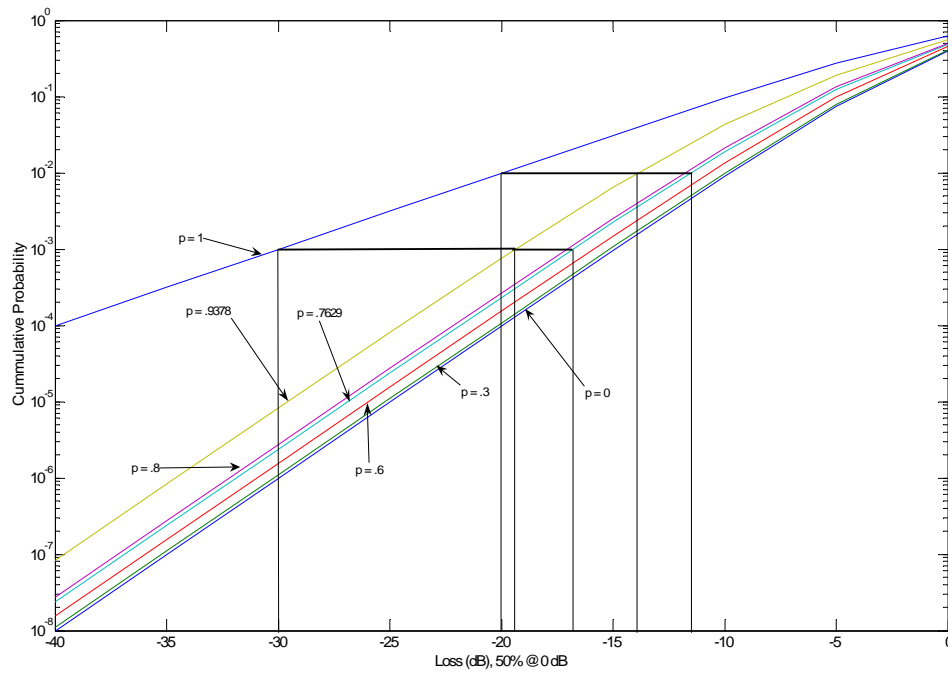


Figure B.1. Two element selection diversity fade probability

APPENDIX C: POWER SUPPLY DESIGN FOR CHAPTER 6

For the IPSN 2007 conference (detailed in Chapter 6), a MATLAB GUI was created to communicate with a wireless node; this node, in turn, communicated remotely with a second node which controlled the antenna phases. As the system was initially designed, the general purpose input/output (GPIO) on the wireless sensor could not supply the requisite negative voltage or the current for the phase shifter. Due to this limitation, an additional power supply was constructed.

Pictured in Figure C.1 are three version of the power supply for the antenna. The box on the left is the first generation and the box on the right is the latest. The first version of the power supply was built to change the phases of the phase shifter by throwing one of the three switches, each corresponding to 45° , 90° , or 180° . The box also contained two 9 V batteries along with two voltage regulators to supply the positive and negative 5 V required by the antenna. The next generation, picture in the center of Figure C.1, automated phase shifting by taking control signals from the GPIO of a wireless node.

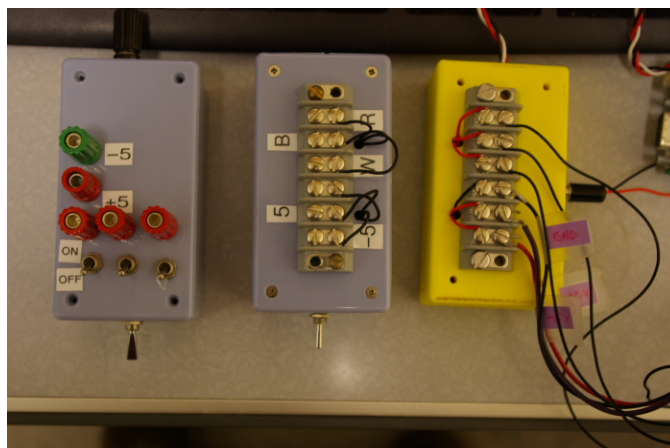


Figure C.1. Three power supply generations (oldest to newest, from left to right)



Figure C.2. Latest version of antenna power supply

The latest version of the power supply, depicted above in Figure C.2, also has fully automated phase shifting via control lines connected to the GPIO of the wireless sensor node. The device no longer depends on the two bulky 9 volt batteries, instead taking power from the node power supply. Rather than using two voltage regulators, a DC-DC converter IC from Maxim was used in conjunction with a negative voltage regulator to supply the positive and negative supplies. The GPIO lines interfaced with

three low current relays which supplied the voltage and current necessary to change the antenna phase shift.

Figure C.3 shows that much of the space on the prototype's circuit board is unused, indicating that the power supply could be more compact and would be relatively simple to integrate onto a wireless sensor node. As proofs of concept, the prototype antennas and power supply certainly work, though further work to find lower power components is suggested.

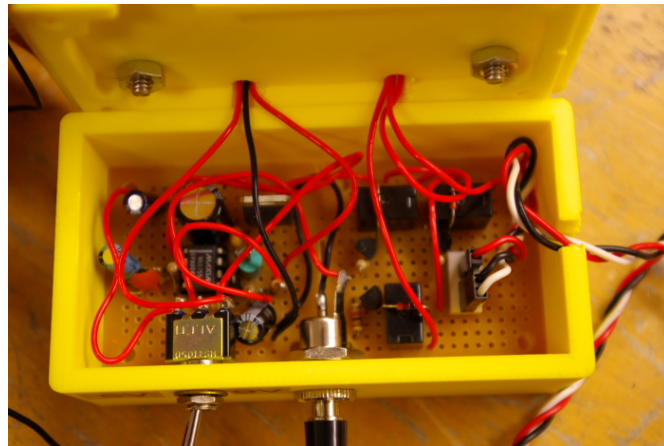


Figure C.3. Power supply circuit board

Figure C.4 depicts the schematic for the power supply pictured in Figure C.3. The device supplies 5V at 1 Amp and -5 V at .2 A. A Maxim 755 DC-DC inverter supplies -5 V using a 160 kHz switching frequency – well below the 2.4 GHz ISM band of interest. The power supply also converts the 3.3V low current logic signals from the microcontroller to 5V with an output current ranging from .33 A to 1 A. The schematic in Figure C.4 can readily undergo a number of changes to make it more fitting for

integration with a wireless sensor platform. For example, the 5 V regulator supplies more than enough current at 1 amp and should be replaced with a 5V Buck converter. Also, the power supply could be made of surface mount parts instead of through-hole and more strategically placed for efficient space usage.

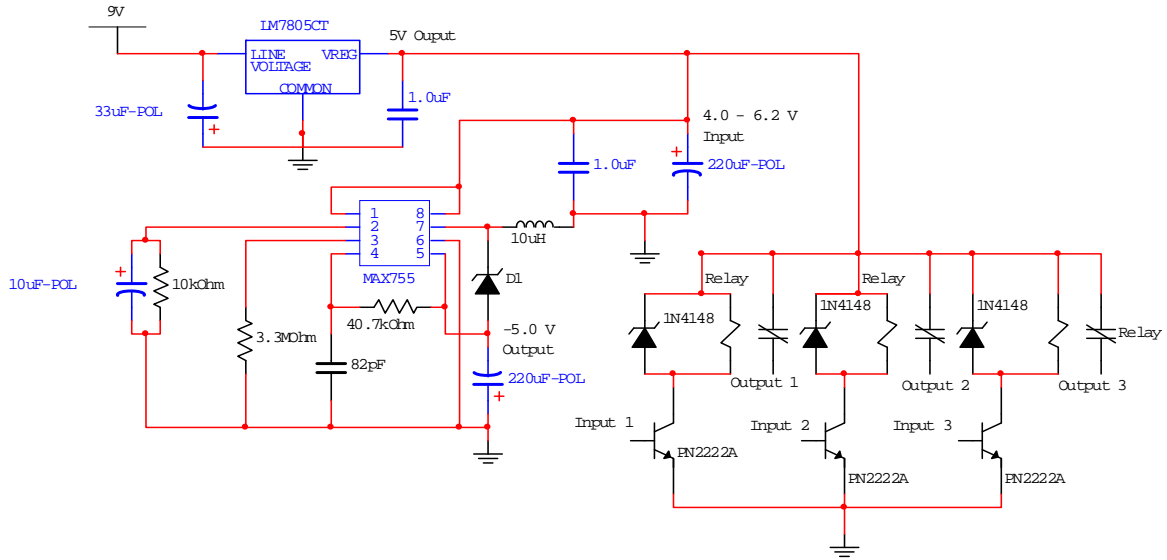


Figure C.4. Schematic for power supply in C.3.

The power supply provides three different voltages: 5 Volts, -5 Volts, and ground. The 5 Volt source is used to power the switch which connects one of three paths (left element, right element, or combined path) to the output terminal. The -5 Volt source is used to supply the phase shifter. Both the switch and the phase shifter require logic signals to operate. Although the combined path was used by default, the node could, ostensibly, switch between the three paths. Instead, the simpler form of diversity was used where only the logic inputs (0 or 5 Volts) to the phase shifter were toggled. The

Freescale board was capable of supplying 3 Volts maximum (2.8 Volts, typically) which would be considered a very low logic 1 by the phase shifter. For the purpose of our experiments, the antenna needed a solid logic 1 such that it would be certain that the phase shifter was receiving the appropriate signals. Accordingly, the power supply uses three relays to adjust the voltage range from 0 to 3 Volts to 0 to 5 Volts, giving both a solid logic 1 and logic 0.